Chapter 10
Fluid-Structure Interaction

Simulating a flow in time dependent domains is a significant part of fluid-structure interaction. It plays an important role in many disciplines. We mention, for example, construction of airplanes (vibrations of wings) or turbines (vibrations of blades), some problems in civil engineering (interaction of wind with constructions of bridges, TV towers or cooling towers of power stations), car industry (vibrations of various elements of a coachwork), but also in medicine (haemodynamics or flow of air in vocal folds). In a number of these examples the moving medium is a gas and the flow is compressible. For low Mach number flows, incompressible models are often used (as e.g., in [266]), but in some cases compressibility plays an important role.

In this chapter we describe the discontinuous Galerkin method applied to the numerical solution of compressible flow in time dependent domains and present some applications to problems in fluid-structure interaction. The main ingredient of this technique is the ALE (arbitrary Lagrangian–Eulerian) formulation of the compressible Navier–Stokes equations, which is discretized by modifying the DGM described in the previous chapter.

10.1 Formulation of Flow in a Time-Dependent Domain

We will be concerned with the numerical solution of a compressible flow in a bounded domain $\Omega_t \subset \mathbb{R}^d$ ($d = 2$ or 3) depending on time $t \in [0, T]$, $0 < T < \infty$. We start from the system of the compressible Navier–Stokes equations written in the dimensionless form (9.12), i.e.,

$$\frac{\partial \boldsymbol{w}}{\partial t} + \sum_{s=1}^{d} \frac{\partial \boldsymbol{f}_s(\boldsymbol{w})}{\partial x_s} = \sum_{s=1}^{d} \frac{\partial \boldsymbol{R}_s(\boldsymbol{w}, \nabla \boldsymbol{w})}{\partial x_s} \quad \text{in } Q_T, \tag{10.1}$$

V. Dolejší and M. Feistauer, *Discontinuous Galerkin Method*,
Springer Series in Computational Mathematics 48,
DOI 10.1007/978-3-319-19267-3_10

where we set $Q_T = \{(x,t);\ x \in \Omega_t,\ t \in (0,T)\}$. We use the notation (9.13)–(9.33) from Chap. 9.

In order to take into account the time dependence of the domain, we use the *arbitrary Lagrangian-Eulerian (ALE) method*, proposed, e.g., in [229]. We define a *reference domain* Ω_0 (also called reference configuration) and introduce a regular one-to-one *ALE mapping* of Ω_0 onto the *current configuration* Ω_t (cf. [229], [266] and [272])

$$\mathrm{A}_t : \overline{\Omega}_0 \longrightarrow \overline{\Omega}_t, \text{ i.e., } X \in \overline{\Omega}_0 \longmapsto x = x(X,t) = \mathrm{A}_t(X) \in \overline{\Omega}_t.$$

Here we use the notation X for points in $\overline{\Omega}_0$ and $x = x(X,t)$ for points in $\overline{\Omega}_t$.

Further, we define the *domain velocity*:

$$\tilde{z}(X,t) = \frac{\partial}{\partial t}\mathrm{A}_t(X), \quad t \in [0,T],\ X \in \Omega_0,$$
$$z(x,t) = \tilde{z}(\mathrm{A}_t^{-1}(x),t), \quad t \in [0,T],\ x \in \Omega_t,$$

and the *ALE derivative* of a function $f = f(x,t)$ defined for $x \in \Omega_t$ and $t \in [0,T]$:

$$\frac{\mathrm{D}^{\mathrm{A}}}{\mathrm{D}t} f(x,t) = \frac{\partial \tilde{f}}{\partial t}(X,t), \tag{10.2}$$

where

$$\tilde{f}(X,t) = f(\mathrm{A}_t(X),t),\ X \in \Omega_0,\ x = \mathrm{A}_t(X). \tag{10.3}$$

As a direct consequence of the chain rule we get the relation

$$\frac{\mathrm{D}^{\mathrm{A}} f}{\mathrm{D}t} = \frac{\partial f}{\partial t} + \nabla \cdot (zf) - f\,\nabla \cdot z.$$

This leads to the *ALE formulation of the Navier–Stokes equations*

$$\frac{\mathrm{D}^{\mathrm{A}} \boldsymbol{w}}{\mathrm{D}t} + \sum_{s=1}^{d} \frac{\partial \boldsymbol{g}_s(\boldsymbol{w})}{\partial x_s} + \boldsymbol{w}\,\nabla \cdot \boldsymbol{z} = \sum_{s=1}^{d} \frac{\partial \boldsymbol{R}_s(\boldsymbol{w}, \nabla \boldsymbol{w})}{\partial x_s}, \tag{10.4}$$

where

$$\boldsymbol{g}_s(\boldsymbol{w}) := \boldsymbol{f}_s(\boldsymbol{w}) - z_s \boldsymbol{w}, \quad s = 1, \ldots, d, \tag{10.5}$$

are the *ALE modified inviscid fluxes*. We see that the partial time derivative $\partial/\partial t$ in (10.1) is replaced by the ALE derivative $\mathrm{D}^{\mathrm{A}}/\mathrm{D}t$, the inviscid Euler fluxes $\boldsymbol{f}_s(\boldsymbol{w})$ are replaced by the ALE modified inviscid fluxes $\boldsymbol{g}_s(\boldsymbol{w})$ and new linear reaction term $\boldsymbol{w}\,\nabla \cdot \boldsymbol{z}$ appears in (10.4).

System (10.4) is equipped with the initial condition

$$\boldsymbol{w}(x,0) = \boldsymbol{w}^0(x), \quad x \in \Omega_0, \tag{10.6}$$

and boundary conditions similar to (9.35)–(9.37). We assume that $\partial\Omega_t = \partial\Omega_i \cup \partial\Omega_o \cup \partial\Omega_{W_t}$ is a disjoint partition of the boundary $\partial\Omega_t$, where the inlet $\partial\Omega_i$ and outlet $\partial\Omega_o$ are independent of time and the set $\partial\Omega_{W_t}$ represents impermeable walls, whose part may move in dependence on time. We prescribe the boundary conditions

$$\rho = \rho_D, \ \ \boldsymbol{v} = \boldsymbol{v}_D, \ \sum_{k=1}^{d}\left(\sum_{l=1}^{d}\tau_{lk}^{\mathrm{V}} n_l\right)v_k + \frac{\gamma}{\mathrm{Re}\,\mathrm{Pr}}\frac{\partial\theta}{\partial\boldsymbol{n}} = 0 \quad \text{on } \partial\Omega_i, \tag{10.7}$$

$$\sum_{k=1}^{d}\tau_{sk}^{\mathrm{V}} n_k = 0, \ s = 1,\dots,d, \quad \frac{\partial\theta}{\partial\boldsymbol{n}} = 0 \quad \text{on } \partial\Omega_o, \tag{10.8}$$

$$\boldsymbol{v} = \boldsymbol{z}_D, \ \frac{\partial\theta}{\partial\boldsymbol{n}} = 0 \quad \text{on } \partial\Omega_{W_t}, \tag{10.9}$$

where ρ_D, $\boldsymbol{v}_D$ and $\boldsymbol{z}_D$ are given functions and $\boldsymbol{n} = (n_1,\dots,n_d)$ is an outer unit normal to $\partial\Omega_t$. The vector function $\boldsymbol{z}_D$ represents the velocity of the moving wall.

10.1.1 Space Discretization of the Flow Problem

For the space semidiscretization we use the discontinuous Galerkin method. We proceed in a similar way as in the previous chapter. We construct a polygonal (or polyhedral) approximation Ω_{ht} of the domain Ω_t. The parts $\partial\Omega_i$, $\partial\Omega_o$ and $\partial\Omega_{W_t}$ of the boundary $\partial\Omega_t$ are approximated by parts $\partial\Omega_{hi}$, $\partial\Omega_{ho}$ and $\partial\Omega_{hW_t}$, respectively, of $\partial\Omega_{ht}$. By $\mathscr{T}_{ht}$ we denote a partition of the closure $\overline{\Omega}_{ht}$ of the domain Ω_{ht} into a finite number of closed simplexes K with mutually disjoint interiors such that $\overline{\Omega}_{ht} = \bigcup_{K\in\mathscr{T}_{ht}} K$. By $\mathscr{F}_{ht}$ we denote the system of all faces of all elements $K \in \mathscr{T}_{ht}$. Further, we introduce the set of boundary faces $\mathscr{F}_{ht}^B = \{\Gamma \in \mathscr{F}_{ht};\ \Gamma \subset \partial\Omega_{ht}\}$, the set of "Dirichlet" boundary faces $\mathscr{F}_{ht}^D = \left\{\Gamma \in \mathscr{F}_{ht}^B;\ \text{a Dirichlet condition is given on } \Gamma\right\}$ and the set of inner faces $\mathscr{F}_{ht}^I = \mathscr{F}_{ht} \setminus \mathscr{F}_{ht}^B$. Moreover, in $\mathscr{F}_{ht}^B$ we distinguish the sets $\mathscr{F}_{ht}^i$, $\mathscr{F}_{ht}^o$ and $\mathscr{F}_{ht}^W$ of all inlet, outlet and wall faces, respectively, and put $\mathscr{F}_{ht}^{io} = \mathscr{F}_{ht}^i \cup \mathscr{F}_{ht}^o$.

Each $\Gamma \in \mathscr{F}_{ht}$ is associated with a unit vector $\boldsymbol{n}_\Gamma$ normal to Γ. For $\Gamma \in \mathscr{F}_{ht}^B$ the normal $\boldsymbol{n}_\Gamma$ has the same orientation as the outer normal to $\partial\Omega_{ht}$. We set $d(\Gamma) =$ diameter of $\Gamma \in \mathscr{F}_{ht}$. For each $\Gamma \in \mathscr{F}_{ht}^I$ there exist two neighbouring elements $K_\Gamma^{(L)}, K_\Gamma^{(R)} \in \mathscr{T}_{ht}$ such that $\Gamma \subset \partial K_\Gamma^{(R)} \cap \partial K_\Gamma^{(L)}$. We use the convention that $K_\Gamma^{(R)}$ lies in the direction of $\boldsymbol{n}_\Gamma$ and $K_\Gamma^{(L)}$ lies in the opposite direction to $\boldsymbol{n}_\Gamma$. If $\Gamma \in \mathscr{F}_{ht}^B$, then the element adjacent to Γ will be denoted by $K_\Gamma^{(L)}$.

The approximate solution will be sought in the space of piecewise polynomial functions

$$\boldsymbol{S}_{hpt} = (S_{hpt})^{d+2}, \quad \text{with } S_{hpt} = \{v;\, v|_K \in P_p(K)\ \forall\, K \in \mathscr{T}_{ht}\}, \tag{10.10}$$

where $p > 0$ is an integer and $P_p(K)$ denotes the space of all polynomials on K of degree $\le p$. For any function $\boldsymbol{\varphi} \in \boldsymbol{S}_{hpt}$ and any face $\Gamma \in \mathscr{F}_{ht}$ we use the standard symbols $\boldsymbol{\varphi}_\Gamma^{(L)}$, and $\boldsymbol{\varphi}_\Gamma^{(R)}$, $\langle \boldsymbol{\varphi} \rangle_\Gamma$ and $[\boldsymbol{\varphi}]_\Gamma$. (See e.g., Sect. 9.2.1.)

The discrete problem is derived in a standard way: We multiply system (10.4) by a test function $\boldsymbol{\varphi}_h \in \boldsymbol{S}_{hpt}$, integrate over $K \in \mathscr{T}_{ht}$, apply Green's theorem, sum over all elements $K \in \mathscr{T}_{ht}$, use the concept of the numerical flux and introduce suitable mutually vanishing terms for a regular exact solution. Moreover, we carry out a linearization of nonlinear terms. Similarly as in Sects. 9.3.2 and 8.4.3, we introduce the partially linearized forms $\hat{\boldsymbol{a}}_h$, $\hat{\boldsymbol{J}}_h^\sigma$, $\boldsymbol{\beta}_h$ and $\boldsymbol{\gamma}_h$, depending now, of course, on time t. The forms $\hat{\boldsymbol{a}}_h$ and $\hat{\boldsymbol{J}}_h^\sigma$ are defined in the same way as in (9.77), (9.78), (9.91) and (9.92), (9.80), (9.81), respectively. For each $t \in I_m$, $m = 1, \dots, r$, we get the viscous form

$$\begin{aligned}
\hat{\boldsymbol{a}}_h(\bar{\boldsymbol{w}}_h, \boldsymbol{w}_h, \boldsymbol{\varphi}_h, t) = {} & \sum_{K \in \mathscr{T}_{ht}} \int_K \sum_{s,k=1}^{d} \left(\mathbb{K}_{s,k}(\bar{\boldsymbol{w}}_h) \frac{\partial \boldsymbol{w}_h}{\partial x_k} \right) \cdot \frac{\partial \boldsymbol{\varphi}_h}{\partial x_s} \, \mathrm{d}x \\
& - \sum_{\Gamma \in \mathscr{F}_{ht}^I} \int_\Gamma \sum_{s=1}^{d} \left\langle \sum_{k=1}^{d} \mathbb{K}_{s,k}(\bar{\boldsymbol{w}}_h) \frac{\partial \boldsymbol{w}_h}{\partial x_k} \right\rangle n_s \cdot [\boldsymbol{\varphi}_h] \, \mathrm{d}S \\
& - \sum_{\Gamma \in \mathscr{F}_{ht}^i} \int_\Gamma \sum_{s,k=1}^{d} \mathbb{K}_{s,k}(\bar{\boldsymbol{w}}_h) \frac{\partial \boldsymbol{w}_h}{\partial x_k} n_s \cdot \boldsymbol{\varphi}_h \, \mathrm{d}S \\
& - \sum_{\Gamma \in \mathscr{F}_{ht}^W} \int_\Gamma \sum_{s,k=1}^{d} \mathbb{K}_{s,k}^W(\bar{\boldsymbol{w}}_h) \frac{\partial \boldsymbol{w}_h}{\partial x_k} n_s \cdot \boldsymbol{\varphi}_h \, \mathrm{d}S \\
& - \Theta \left(\sum_{\Gamma \in \mathscr{F}_{ht}^I} \int_\Gamma \sum_{s,k=1}^{d} \left\langle \mathbb{K}_{s,k}^{\mathrm{T}}(\bar{\boldsymbol{w}}_h) \frac{\partial \boldsymbol{\varphi}_h}{\partial x_k} \right\rangle n_s \cdot [\boldsymbol{w}_h] \, \mathrm{d}S \right. \\
& \quad + \sum_{\Gamma \in \mathscr{F}_{ht}^i} \int_\Gamma \sum_{s,k=1}^{d} \mathbb{K}_{s,k}^{\mathrm{T}}(\bar{\boldsymbol{w}}_h) \frac{\partial \boldsymbol{\varphi}_h}{\partial x_k} n_s \cdot (\boldsymbol{w}_h - \bar{\boldsymbol{w}}_B) \, \mathrm{d}S \\
& \quad \left. + \sum_{\Gamma \in \mathscr{F}_{ht}^W} \int_\Gamma \sum_{s,k=1}^{d} \left(\mathbb{K}_{s,k}^W(\bar{\boldsymbol{w}}_h) \right)^{\mathrm{T}} \frac{\partial \boldsymbol{\varphi}_h}{\partial x_k} n_s \cdot (\boldsymbol{w}_h - \bar{\boldsymbol{w}}_B) \, \mathrm{d}S \right).
\end{aligned} \tag{10.11}$$

The parameter Θ can attain the values 1, 0 and -1 for the SIPG, IIPG and NIPG version, respectively. Moreover, the penalty form now reads

$$\hat{\boldsymbol{J}}_h^{\sigma}(\bar{\boldsymbol{w}}_h, \boldsymbol{w}_h, \boldsymbol{\varphi}_h, t) = \sum_{\Gamma \in \mathscr{F}_{ht}^I} \int_\Gamma \sigma[\boldsymbol{w}_h] \cdot [\boldsymbol{\varphi}_h] \,\mathrm{d}S + \sum_{\Gamma \in \mathscr{F}_{ht}^i} \int_\Gamma \sigma(\boldsymbol{w}_h - \bar{\boldsymbol{w}}_B) \cdot \boldsymbol{\varphi}_h \,\mathrm{d}S$$
$$+ \sum_{\Gamma \in \mathscr{F}_{ht}^W} \int_\Gamma \sigma(\boldsymbol{w}_h - \bar{\boldsymbol{w}}_B) \cdot \mathscr{V}(\boldsymbol{\varphi}_h) \,\mathrm{d}S \tag{10.12}$$

where the operator $\mathscr{V}$ is defined by (9.66). The weight σ in $\hat{\boldsymbol{J}}_h^{\sigma}$ is defined by (9.67). The boundary state $\bar{\boldsymbol{w}}_B$ is obtained on the basis of the Dirichlet boundary conditions in (10.7) and (10.9) and extrapolation:

$$\bar{\boldsymbol{w}}_B|_\Gamma = (\rho_D, \rho_D v_{D1}, \rho_D v_{D2}, c_v \rho_D \bar{\theta}_\Gamma^{(L)} + \frac{1}{2}\rho_D |\boldsymbol{v}_D|^2), \quad \Gamma \subset \partial\Omega_i, \tag{10.13}$$

$$\bar{\boldsymbol{w}}_B|_\Gamma = \bar{\boldsymbol{w}}_\Gamma^{(L)}, \quad \Gamma \subset \partial\Omega_o, \tag{10.14}$$

$$\bar{\boldsymbol{w}}_B|_\Gamma = (\bar{\rho}_\Gamma^{(L)}, \bar{\rho}_\Gamma^{(L)} z_{D1}, \bar{\rho}_\Gamma^{(L)} z_{D2}, c_v \bar{\rho}_\Gamma^{(L)} \bar{\theta}_\Gamma^{(L)} + \frac{1}{2}\bar{\rho}_\Gamma^{(L)} |\boldsymbol{z}_D|^2), \quad \Gamma \subset \partial\Omega_{W_t}. \tag{10.15}$$

The quantities $\bar{\rho}, \bar{\theta}$, etc. correspond to the state $\bar{\boldsymbol{w}}_h$. We see that as in (9.63) it is possible to write $\bar{\boldsymbol{w}}_B = BC(\bar{\boldsymbol{w}}_h, \boldsymbol{u}_D)$, where $\boldsymbol{u}_D$ represents the Dirichlet data.

Further, we define the reaction form

$$\boldsymbol{d}_h(\boldsymbol{w}_h, \boldsymbol{\varphi}_h, t) = \sum_{K \in \mathscr{T}_{ht}} \int_K (\boldsymbol{w}_h \cdot \boldsymbol{\varphi}_h) \nabla \cdot \boldsymbol{z} \,\mathrm{d}x. \tag{10.16}$$

In order to avoid spurious oscillations in the approximate solution in the vicinity of discontinuities or steep gradients, we apply local artificial viscosity forms. They are based on the discontinuity indicator

$$g_t(K) = \int_{\partial K} [\bar{w}_{h,1}^k]^2 \,\mathrm{d}S / (h_K |K|^{3/4}), \quad K \in \mathscr{T}_{ht}, \tag{10.17}$$

introduced in (8.178). By $[\bar{w}_{h,1}^k]$ we denote the jump of the density function $\bar{w}_{h,1}^k = \bar{\rho}_h$ on the boundary ∂K, corresponding to the state $\bar{w}_h$, and $|K|$ denotes the volume of the element K. Then we define the discrete discontinuity indicator

$$G_t(K) = 0 \ \text{ if } g_t(K) < 1, \quad G_t(K) = 1 \ \text{ if } g_t(K) \geq 1, \quad K \in \mathscr{T}_{ht}, \tag{10.18}$$

and the artificial viscosity forms defined in analogy to (8.181) and (8.182):

$$\boldsymbol{\beta}_h(\bar{\boldsymbol{w}}_h, \boldsymbol{w}_h, \boldsymbol{\varphi}_h, t) = \nu_1 \sum_{K \in \mathcal{T}_{ht}} h_K G_t(K) \int_K \nabla \boldsymbol{w}_h \cdot \nabla \boldsymbol{\varphi}_h \,\mathrm{d}x, \tag{10.19}$$

$$\boldsymbol{\gamma}_h(\bar{\boldsymbol{w}}_h, \boldsymbol{w}_h, \boldsymbol{\varphi}_h, t) = \nu_2 \sum_{\Gamma \in \mathcal{F}_{ht}^I} \frac{1}{2}\big(G_t(K_\Gamma^{(L)}) + G_t(K_\Gamma^{(R)})\big) \int_\Gamma [\boldsymbol{w}_h] \cdot [\boldsymbol{\varphi}_h] \,\mathrm{d}S,$$

with parameters $\nu_1,\ \nu_2 = O(1)$. It is also possible to use more sophisticated local artificial viscosity forms defined in an analogous way as in (8.180), (8.183) and (8.184).

Special attention has to be paid to the convection form $\hat{\boldsymbol{b}}_h$. Denoting by $\mathbb{I}$ the unit matrix and taking into account the definition of $\boldsymbol{g}_s$ in (10.5) and notation (8.14), we have

$$\frac{\mathrm{D}\boldsymbol{g}_s(\boldsymbol{w})}{\mathrm{D}\boldsymbol{w}} = \frac{\mathrm{D}\boldsymbol{f}_s(\boldsymbol{w})}{\mathrm{D}\boldsymbol{w}} - z_s\mathbb{I} = \mathbb{A}_s(\boldsymbol{w}) - z_s\mathbb{I}, \tag{10.20}$$

and can write

$$\mathbb{P}_g(\boldsymbol{w}, \boldsymbol{n}) = \sum_{s=1}^{d} \frac{\mathrm{D}\boldsymbol{g}_s(\boldsymbol{w})}{\mathrm{D}\boldsymbol{w}} n_s = \sum_{s=1}^{d} (\mathbb{A}_s(\boldsymbol{w}) n_s - z_s n_s \mathbb{I})\,.$$

By Lemma 8.6 (namely, relation (8.29)), this matrix is diagonalizable. It means that there exists a nonsingular matrix $\mathbb{T} = \mathbb{T}(\boldsymbol{w}, \boldsymbol{n})$ such that

$$\mathbb{P}_g = \mathbb{T}^{-1}\boldsymbol{\Lambda}\mathbb{T}, \quad \boldsymbol{\Lambda} = \mathrm{diag}(\lambda_1, \ldots, \lambda_{d+2}),$$

where $\lambda_i = \lambda_i(\boldsymbol{w}, \boldsymbol{n})$ are eigenvalues of the matrix $\mathbb{P}_g$. By virtue of (8.29), (8.30) and (10.20),

$$\begin{aligned} &\lambda_1(\boldsymbol{w}, \boldsymbol{n}) = (\boldsymbol{v} - \boldsymbol{z}) \cdot \boldsymbol{n} - a, \\ &\lambda_2(\boldsymbol{w}, \boldsymbol{n}) = \cdots = \lambda_{d+1}(\boldsymbol{w}, \boldsymbol{n}) = (\boldsymbol{v} - \boldsymbol{z}) \cdot \boldsymbol{n}, \\ &\lambda_{d+2}(\boldsymbol{w}, \boldsymbol{n}) = (\boldsymbol{v} - \boldsymbol{z}) \cdot \boldsymbol{n} + a. \end{aligned} \tag{10.21}$$

Now we define the "positive and negative" parts of the matrix $\mathbb{P}_g$ by

$$\mathbb{P}_g^{\pm} = \mathbb{T}^{-1}\boldsymbol{\Lambda}^{\pm}\mathbb{T}, \quad \boldsymbol{\Lambda}^{\pm} = \mathrm{diag}(\lambda_1^{\pm}, \ldots, \lambda_{d+2}^{\pm}),$$

where $\lambda^+ = \max(\lambda, 0),\ \lambda^- = \min(\lambda, 0)$. Using the above concepts, for arbitrary states $\boldsymbol{w}^L$, $\boldsymbol{w}^R$ and a unit 2D vector $\boldsymbol{n}$, we introduce the ALE modified Vijayasundaram numerical flux (cf. Sect. 8.4.3)

$$\mathbf{H}_g(\boldsymbol{w}_L, \boldsymbol{w}_R, \boldsymbol{n}) = \mathbb{P}_g^+\Big(\frac{\boldsymbol{w}_L + \boldsymbol{w}_R}{2}, \boldsymbol{n}\Big)\boldsymbol{w}_L + \mathbb{P}_g^-\Big(\frac{\boldsymbol{w}_L + \boldsymbol{w}_R}{2}, \boldsymbol{n}\Big)\boldsymbol{w}_R. \tag{10.22}$$

On the basis of the above considerations, we can introduce the convection form defined for $\bar{\boldsymbol{w}}_h, \boldsymbol{w}_h, \boldsymbol{\varphi}_h \in \boldsymbol{S}_{hpt}$:

$$\begin{aligned}\hat{\boldsymbol{b}}_h(\bar{\boldsymbol{w}}_h, \boldsymbol{w}_h, \boldsymbol{\varphi}_h, t) = &- \sum_{K\in\mathscr{T}_{ht}} \int_K \sum_{s=1}^{d} ((\mathbb{A}_s(\bar{\boldsymbol{w}}_h) - z_s\mathbb{I})\boldsymbol{w}_h) \cdot \frac{\partial \boldsymbol{\varphi}_h}{\partial x_s}\,\mathrm{d}x \\ &+ \sum_{\Gamma\in\mathscr{F}_{ht}^I} \int_\Gamma \left(\mathbb{P}_g^+\left(\langle\bar{\boldsymbol{w}}_h\rangle_\Gamma, \boldsymbol{n}_\Gamma\right)\boldsymbol{w}_{h\Gamma}^{(L)} + \mathbb{P}_g^-\left(\langle\bar{\boldsymbol{w}}_h\rangle_\Gamma, \boldsymbol{n}_\Gamma\right)\boldsymbol{w}_{h\Gamma}^{(R)}\right)\cdot\boldsymbol{\varphi}_h \mathrm{d}S \\ &+ \sum_{\Gamma\in\mathscr{F}_{ht}^W} \int_\Gamma \boldsymbol{f}_W(\bar{\boldsymbol{w}}_{h\Gamma}^{(L)}, \boldsymbol{n}_\Gamma)\cdot\boldsymbol{\varphi}_h\,\mathrm{d}S \\ &+ \sum_{\Gamma\mathscr{F}_{ht}^{io}} \int_\Gamma \left(\mathbb{P}_g^+(\bar{\boldsymbol{w}}_{h\Gamma}^{(L)}, \boldsymbol{n}_\Gamma)\boldsymbol{w}_{h\Gamma}^{(L)} + \mathbb{P}_g^-(\bar{\boldsymbol{w}}_{h\Gamma}^{(L)}, \boldsymbol{n}_\Gamma)\mathscr{B}(\bar{\boldsymbol{w}}_\Gamma^{(L)}, \boldsymbol{w}_{\mathrm{BC}})\right)\cdot\boldsymbol{\varphi}_h \mathrm{d}S.\end{aligned} \tag{10.23}$$

The symbol $\boldsymbol{f}_W$ denotes the boundary flux on the approximation $\partial\Omega_{hW_t}$ of the impermeable moving wall. We proceed here in a different way than in Sect. 8.3.1. On every face $\Gamma \in \mathscr{F}_{ht}^W$ (with the normal $\boldsymbol{n} = \boldsymbol{n}_\Gamma$) we use the relation

$$\sum_{s=1}^{d} \boldsymbol{g}_s(\boldsymbol{w})n_s = \begin{pmatrix} \rho(\boldsymbol{v} - \boldsymbol{z}_D)\cdot\boldsymbol{n} \\ \rho v_1(\boldsymbol{v} - \boldsymbol{z}_D)\cdot\boldsymbol{n} + \mathrm{p}n_1 \\ \vdots \\ \rho v_d(\boldsymbol{v} - \boldsymbol{z}_D)\cdot\boldsymbol{n} + \mathrm{p}n_d \\ E(\boldsymbol{v} - \boldsymbol{z}_D)\cdot\boldsymbol{n} + \mathrm{p}\boldsymbol{z}_D\cdot\boldsymbol{n} \end{pmatrix}, \tag{10.24}$$

which follows from (10.5) and (8.10). In view of (10.9), $\boldsymbol{v} = \boldsymbol{z}_D$ on $\Gamma \in \mathscr{F}_{ht}^W$, and hence

$$\sum_{s=1}^{d} \boldsymbol{g}_s(\boldsymbol{w})n_s = \mathrm{p}(0, n_1, \ldots, n_d, \boldsymbol{z}_D\cdot\boldsymbol{n})^{\mathrm{T}}. \tag{10.25}$$

This leads us to the choice of boundary flux on $\partial\Omega_{hW_t}$ in the form

$$\boldsymbol{f}_W(\bar{\boldsymbol{w}}_{h\Gamma}^{(L)}, \boldsymbol{n}_\Gamma) = \bar{\mathrm{p}}_{h\Gamma}^{(L)}(0, n_1, \ldots, n_d, \boldsymbol{z}_D\cdot\boldsymbol{n})^{\mathrm{T}}, \tag{10.26}$$

where $\bar{\mathrm{p}}_{h\Gamma}^{(L)}$ is the trace of the pressure on $\Gamma \in \mathscr{F}_{ht}^W$, corresponding to the function $\bar{\boldsymbol{w}}_{h\Gamma}^{(L)}$.

10.1.2 Time Discretization by the BDF Method

Let us construct a partition $0 = t_0 < t_1 < t_2 < \cdots < t_r = T$ of the time interval $[0, T]$ and define the time step $\tau_n = t_n - t_{n-1}$. We use the approximations $\boldsymbol{w}_h(t_n) \approx \boldsymbol{w}_h^n \in \boldsymbol{S}_{hpt_n}$, $\boldsymbol{z}(t_n) \approx \boldsymbol{z}^n$, $n = 0, 1, \ldots$ Let us assume that $\boldsymbol{w}_h^n$, $n = 0, \ldots, m-1$, are already known and we want to determine $\boldsymbol{w}_h^m$. We introduce the functions

$$\hat{\boldsymbol{w}}_h^n = \boldsymbol{w}_h^n \circ \mathrm{A}_{t_n} \circ \mathrm{A}_{t_m}^{-1}, \quad n = m, m-1, m-2, \ldots, \tag{10.27}$$

i.e.,

$$\hat{\boldsymbol{w}}_h^n(x) = \boldsymbol{w}_h^n(\mathrm{A}_{t_n}(\mathrm{A}_{t_m}^{-1}(x))), \quad x \in \Omega_{t_m}. \tag{10.28}$$

Obviously, for $n = m$, the definition of $\hat{\boldsymbol{w}}_h^m$ by (10.27) is trivial, since

$$\hat{\boldsymbol{w}}_h^m(x) = \boldsymbol{w}_h^m(x), \quad x \in \Omega_{t_m}. \tag{10.29}$$

The transformation of $\boldsymbol{w}_h^n$ from the domain Ω_{t_n} to Ω_0 reads

$$\tilde{\boldsymbol{w}}_h^n(X) = \boldsymbol{w}_h^n(\mathrm{A}_{t_n}(X)), \quad X \in \Omega_0. \tag{10.30}$$

Then

$$\hat{\boldsymbol{w}}_h^n(x) = \tilde{\boldsymbol{w}}_h^n(\mathrm{A}_{t_m}^{-1}(x)), \quad x \in \Omega_{t_m}. \tag{10.31}$$

In order to define the ALE derivative of the exact solution $\boldsymbol{w}$, by virtue of (10.3), we introduce the function

$$\tilde{\boldsymbol{w}}(X, t) = \boldsymbol{w}(\mathrm{A}_t(X), t), \quad X \in \Omega_0, \ t \in [0, T]. \tag{10.32}$$

We use the approximations

$$\boldsymbol{w}(x, t_n) \approx \boldsymbol{w}_h^n(x), \quad x \in \Omega_{t_n}, \tag{10.33}$$

and thus in view of (10.31),

$$\tilde{\boldsymbol{w}}(X, t_n) \approx \tilde{\boldsymbol{w}}_h^n(X) = \hat{\boldsymbol{w}}_h^n(x), \quad X \in \Omega_0, \ X = \mathrm{A}_{t_m}^{-1}(x), \ x \in \Omega_{t_m}. \tag{10.34}$$

Now, by (10.2) and the above relations, we can obtain the approximation of the ALE derivative of the vector function $\boldsymbol{w}$ at time $t = t_m$ and a point $x \in \Omega_{t_m}$ with the aid of the backward finite difference:

$$\frac{\mathrm{D}^{\mathrm{A}}\boldsymbol{w}}{\mathrm{D}t}(x,t_m) = \frac{\partial\tilde{\boldsymbol{w}}}{\partial t}(X,t_m)|_{X=\mathrm{A}_{t_m}^{-1}(x)}$$
$$\approx \frac{\tilde{\boldsymbol{w}}(X,t_m)-\tilde{\boldsymbol{w}}(X,t_{m-1})}{\tau_m} \approx \frac{\tilde{\boldsymbol{w}}^m(X)-\tilde{\boldsymbol{w}}^{m-1}(X)}{\tau_m}.$$

These relations and (10.34) lead to the first-order *BDF approximation of the ALE derivative* in the form

$$\frac{\mathrm{D}^{\mathrm{A}}\boldsymbol{w}}{\mathrm{D}t}(x,t_m) \approx \frac{\boldsymbol{w}^m(x)-\hat{\boldsymbol{w}}^{m-1}(x)}{\tau_m}, \quad x\in\Omega_{t_m}. \tag{10.35}$$

In a similar way the ALE derivative can be approximated by the *backward difference formula* of order q:

$$\frac{\mathrm{D}^{\mathrm{A}}\boldsymbol{w}_h}{\mathrm{D}t}(x,t_m) \approx \frac{\mathrm{D}^{\mathrm{A}}_{appr}\boldsymbol{w}_h}{\mathrm{D}t}(x,t_m) = \frac{1}{\tau_m}\left(\alpha_0\boldsymbol{w}_h^m + \sum_{l=1}^{q}\alpha_l\hat{\boldsymbol{w}}_h^{m-l}(x)\right), \quad x\in\Omega_{t_m}, \tag{10.36}$$

with coefficients $\alpha_l,\ l=0,\dots,q$, depending on $\tau_{m-l},\ l=0,\dots,q-1$, see Sect. 8.4.5. In the beginning of the computation when $m<q$, we approximate the ALE derivative using formulae of the lower order $q:=m$.

In nonlinear terms we use the extrapolation for computing the state $\bar{\boldsymbol{w}}_h^m$:

$$\bar{\boldsymbol{w}}_h^m = \sum_{l=1}^{q}\beta_l\hat{\boldsymbol{w}}_h^{m-l}, \tag{10.37}$$

where $\beta_l,\ l=1,\dots,q$, depend on $\tau_{m-l},\ l=0,\dots,q-1$. If $m<q$, then we apply the extrapolation of order m. The values of the coefficients $\alpha_l, l=0,\dots,q$, and $\beta_l, l=1,\dots,q$, for $q=1,2,3$ are given in Tables 8.2, 8.3 and 8.4, 8.5, respectively.

By the symbol $(\cdot,\cdot)_{t_m}$ we denote the scalar product in $L^2(\Omega_{ht_m})$, i.e.,

$$(\boldsymbol{w}_h,\boldsymbol{\varphi}_h)_{t_m} = \int_{\Omega_{ht_m}}\boldsymbol{w}_h\cdot\boldsymbol{\varphi}_h\,dx. \tag{10.38}$$

Definition 10.1 The sequence of functions $\boldsymbol{w}_h^m\in\boldsymbol{S}_{hpt_m}$, $m=1,2,\dots,r$, is called the approximate solution given by the *ALE BDF-DG scheme* if it satisfies

$$\left(\frac{\mathrm{D}^{\mathrm{A}}_{\mathrm{appr}}\boldsymbol{w}_h}{\mathrm{D}t}(t_m),\boldsymbol{\varphi}_h\right)_{t_m} + \hat{\boldsymbol{a}}_h(\bar{\boldsymbol{w}}_h^m,\boldsymbol{w}_h^m,\boldsymbol{\varphi}_h,t_m) \tag{10.39}$$
$$+\hat{\boldsymbol{b}}_h(\bar{\boldsymbol{w}}_h^m,\boldsymbol{w}_h^m,\boldsymbol{\varphi}_h,t_m)+\hat{\boldsymbol{J}}_h^{\sigma}(\bar{\boldsymbol{w}}_h^m\boldsymbol{w}_h^m,\boldsymbol{\varphi}_h,t_m)+\boldsymbol{d}_h(\boldsymbol{w}_h^m,\boldsymbol{\varphi}_h,t_m)$$
$$+\boldsymbol{\beta}_h(\bar{\boldsymbol{w}}_h^m,\boldsymbol{w}_h^m,\boldsymbol{\varphi}_h,t_m)+\boldsymbol{\gamma}_h(\bar{\boldsymbol{w}}_h^m,\boldsymbol{w}_h^m,\boldsymbol{\varphi}_h,t_m)=0 \qquad \forall\boldsymbol{\varphi}_h\in\boldsymbol{S}_{hpt_m}.$$

10.1.3 Space-Time DG Discretization

Another technique regarding how to construct a method of high-order accuracy both in space and time is the *space-time discontinuous Galerkin method* (ST-DGM). We again consider a partition $0 = t_0 < t_1 < \cdots < t_r = T$ of the time interval $[0, T]$ and denote $I_m = (t_{m-1}, t_m)$, $\overline{I}_m = [t_{m-1}, t_m]$, $\tau_m = t_m - t_{m-1}$, for $m = 1, \ldots, r$. We define the space $\boldsymbol{S}_{h,\tau}^{p,q} = (S_{h,\tau}^{p,q})^{d+2}$, where

$$S_{h,\tau}^{p,q} = \left\{ \phi \,;\, \phi|_{I_m} = \sum_{i=0}^{q} \zeta_i \phi_i, \text{ where } \phi_i \in S_{hpt},\ \zeta_i \in P_q(I_m), m = 1, \ldots, r \right\}$$

with integers $p, q \geq 1$, $P_q(I_m)$ denoting the space of all polynomials in t on I_m of degree $\leq q$ and the space S_{hpt} defined in (10.10). For $\boldsymbol{\varphi} \in \boldsymbol{S}_{h,\tau}^{p,q}$ we introduce the following notation:

$$\boldsymbol{\varphi}_m^{\pm} = \boldsymbol{\varphi}(t_m^{\pm}) = \lim_{t \to t_{m\pm}} \boldsymbol{\varphi}(t), \quad \{\boldsymbol{\varphi}\}_m = \boldsymbol{\varphi}_m^{+} - \boldsymbol{\varphi}_m^{-}. \tag{10.40}$$

Derivation of the discrete problem can be carried out similarly as above. The difference is now that time t is considered continuous, test functions $\boldsymbol{\varphi}_{h\tau} \in \boldsymbol{S}_{h,\tau}^{p,q}$ are used and also the integration over I_m is applied. In order to stick together the solution on intervals I_{m-1} and I_m, we augment the resulting identity by the penalty expression $\left(\{\boldsymbol{w}_{h\tau}\}_{m-1}, \boldsymbol{\varphi}_{h\tau}(t_{m-1}^{+})\right)_{t_{m-1}}$. The initial state $\boldsymbol{w}_{h\tau}(0-) \in S_{h0}^{p}$ is defined as the $L^2(\Omega_{h0})$-projection of $\boldsymbol{w}^0$ on S_{h0}^{p}, i.e.,

$$\left(\boldsymbol{w}_{h\tau}(0-), \boldsymbol{\varphi}_h\right)_{t_0} = \left(\boldsymbol{w}^0, \boldsymbol{\varphi}_h\right)_{t_0} \quad \forall \boldsymbol{\varphi}_h \in \boldsymbol{S}_{hp0}. \tag{10.41}$$

Similarly as in Sect. 10.1.2 we introduce a suitable linearization. We can use two possibilities.
(1) We put $\bar{\boldsymbol{w}}_{h\tau}(t) := \boldsymbol{w}_{h\tau}(t_{m-1}^{-})$ for $t \in I_m$. (This represents a simple time extrapolation.)
(2) Each component of the vector-valued function $\boldsymbol{w}_{h\tau}|_{I_{m-1}}$ is a polynomial in t of degree $\leq q$, and we define the function $\bar{\boldsymbol{w}}_{h\tau}|_{I_m}$ by the time prolongation using values of the polynomial vector function $\boldsymbol{w}_{h\tau}|_{I_{m-1}}$ at time instants $t \in I_m$. Thus, we write $\bar{\boldsymbol{w}}_{h\tau}|_{I_m}(t) := \boldsymbol{w}_{h\tau}|_{I_{m-1}}(t)$ for $t \in I_m$.

Definition 10.2 The *ALE space-time DG (ALE ST-DG) approximate solution* is a function $\boldsymbol{w}_{h\tau}$ satisfying (10.41) and the following conditions:

$$\boldsymbol{w}_{h\tau} \in \boldsymbol{S}_{h,\tau}^{p,q}, \tag{10.42a}$$

$$\int_{I_m} \left(\left(\frac{\mathrm{D}^{\mathrm{A}} \boldsymbol{w}_{h\tau}}{\mathrm{D}t}, \boldsymbol{\varphi}_{h\tau} \right)_t + \hat{\boldsymbol{a}}_h(\bar{\boldsymbol{w}}_{h\tau}, \boldsymbol{w}_{h\tau}, \boldsymbol{\varphi}_{h\tau}, t) \right) \mathrm{d}t \tag{10.42b}$$
$$+ \int_{I_m} \left(\hat{\boldsymbol{b}}_h(\bar{\boldsymbol{w}}_{h\tau}, \boldsymbol{w}_{h\tau}, \boldsymbol{\varphi}_{h\tau}, t) + \hat{\boldsymbol{J}}_h^{\sigma}(\bar{\boldsymbol{w}}_{h\tau}, \boldsymbol{w}_{h\tau}, \boldsymbol{\varphi}_{h\tau}, t) + \boldsymbol{d}_h(\boldsymbol{w}_{h\tau}, \boldsymbol{\varphi}_{h\tau}, t) \right) \mathrm{d}t$$
$$+ \int_{I_m} \left(\boldsymbol{\beta}_h(\bar{\boldsymbol{w}}_{h\tau}, \boldsymbol{w}_{h\tau}, \boldsymbol{\varphi}_{h\tau}, t) + \boldsymbol{\gamma}_h(\bar{\boldsymbol{w}}_{h\tau}, \boldsymbol{w}_{h\tau}, \boldsymbol{\varphi}_{h\tau}, t) \right) \mathrm{d}t$$
$$+ (\{\boldsymbol{w}_{h\tau}\}_{m-1}, \boldsymbol{\varphi}_{h\tau}(t_{m-1}+))_{t_{m-1}} = 0 \quad \forall \boldsymbol{\varphi}_{h\tau} \in \boldsymbol{S}_{h,\tau}^{p,q}, \quad m = 1, ..., r.$$

Remark 10.3 In practical computations, integrals appearing in definitions of the forms $\hat{\boldsymbol{a}}_h$, $\hat{\boldsymbol{b}}_h$, $\boldsymbol{d}_h$, $\hat{\boldsymbol{J}}_h^{\sigma}$, $\boldsymbol{\beta}_h$ and $\boldsymbol{\gamma}_h$ and also the time integrals are evaluated with the aid of quadrature formulae.

The linear algebraic systems equivalent to (10.39) and (10.42) are solved either by the direct solver (e.g., UMFPACK [72]) or by a suitable iteration method (e.g., the GMRES method with block diagonal preconditioning [249].

10.2 Fluid-Structure Interaction

This section is devoted to problems of fluid-structure interaction (FSI). We are concerned with two FSI problems:

- flow-induced airfoil vibrations,
- interaction of compressible flow with elastic structures.

In both cases we deal with 2D models.

10.2.1 Flow-Induced Airfoil Vibrations

In the study of aerodynamical properties of airplane wings or blades of turbines and compressors, the problem of flow-induced airfoil vibrations plays an important role. We consider an *elastically supported airfoil* with two degrees of freedom: the vertical displacement H (positively oriented downwards) and the angle α of rotation around an *elastic axis* EA (positively oriented clockwise), see Fig. 10.1. In this case the boundary of the bounded domain $\Omega_t \subset \mathbb{R}^2$ occupied by gas is formed by three disjoint parts: $\partial\Omega_t = \partial\Omega_i \cup \partial\Omega_o \cup \partial\Omega_{W_t}$, where $\partial\Omega_i$ is the inlet, $\partial\Omega_o$ is the outlet and $\partial\Omega_{W_t}$ denotes the boundary of an airfoil moving in dependence on time.

10.2.1.1 Description of the Airfoil Motion

The motion of the airfoil is described by the system of ordinary differential equations for unknowns H and α:

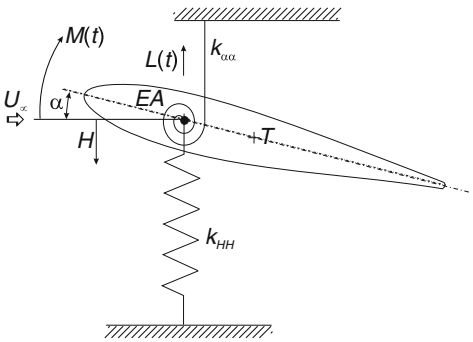

Fig. 10.1 Elastically supported airfoil with two degrees of freedom

$$
\begin{aligned}
& m\ddot{H} + k_{HH}H + S_\alpha\,\ddot{\alpha}\,\cos\alpha - S_\alpha\dot{\alpha}^2\sin\alpha + d_{HH}\dot{H} = -L(t), \\
& S_\alpha\ddot{H}\cos\alpha + I_\alpha\ddot{\alpha} + k_{\alpha\alpha}\alpha + d_{\alpha\alpha}\dot{\alpha} = M(t).
\end{aligned}
\tag{10.43}
$$

The dot and two dots denote the first-order and second-order time derivative, respectively. This system is derived from the Lagrange equations of the second art (see, e.g., [266]). We use the following notation: $L(t)$—aerodynamic lift force (upwards positive), $M(t)$—aerodynamic torsional moment (clockwise positive), m—airfoil mass, S_α—static moment of the airfoil around the elastic axis EA, I_α—inertia moment of the airfoil around the elastic axis EA, k_{HH}—bending stiffness, $k_{\alpha\alpha}$—torsional stiffness, d_{HH}—structural damping in bending, $d_{\alpha\alpha}$—structural damping in torsion, l—airfoil depth (i.e., the length of an airfoil segment in investigation).

System (10.43) is equipped with the initial conditions prescribing the values $H(0), \alpha(0), \dot{H}(0), \dot{\alpha}(0)$. The aerodynamic lift force L acting in the vertical direction and the torsional moment M are defined by

$$
L = -\,l\int_{\partial\Omega_{Wt}}\sum_{j=1}^{2}\tau_{2j}n_j\,\mathrm{d}S, \quad M = l\int_{\partial\Omega_{Wt}}\sum_{i,j=1}^{2}\tau_{ij}n_j r_i^{\mathrm{ort}}\,\mathrm{d}S,
\tag{10.44}
$$

where

$$
\begin{aligned}
& \tau_{ij} = -\mathrm{p}\,\delta_{ij} + \tau_{ij}^V = -\mathrm{p}\,\delta_{ij} + \frac{1}{\mathrm{Re}}\left(\frac{\partial u_i}{\partial x_j} + \frac{\partial u_j}{\partial x_i} - \frac{2}{3}\nabla\cdot\boldsymbol{v}\delta_{ij}\right), \\
& r_1^{\mathrm{ort}} = -(x_2 - x_{EA2}),\ r_2^{\mathrm{ort}} = x_1 - x_{EA1}.
\end{aligned}
\tag{10.45}
$$

By τ_{ij} we denote the components of the aerodynamic stress tensor, δ_{ij} denotes the Kronecker symbol, $\boldsymbol{n} = (n_1, n_2)$ is the unit outer normal to $\partial\Omega_t$ on $\partial\Omega_{Wt}$ (pointing into the airfoil) and $x_{EA} = (x_{EA1}, x_{EA2})$ is the position of the elastic axis (lying in the interior of the airfoil). Relations (10.44) and (10.45) define the coupling of the fluid dynamical model with the structural model.

In contrast to the solution of compressible flow, the numerical solution of the structural problem is not difficult. System (10.43) is transformed to a first-order system and approximated by the Runge-Kutta method. In what follows, we are concerned with the realization of the complete fluid-structure interaction problem.

10.2.1.2 Construction of the ALE Mapping

In the solution of flow-induced airfoil vibrations, for constructing of the ALE mapping the following method can be used. We start from the assumption that we know the airfoil position at time instant t_m, given by the displacement $H(t_m)$ and the rotation angle $\alpha(t_m)$. We want to define the mapping $\mathrm{A}_{t_m} : \overline{\Omega}_{h0} \to \overline{\Omega}_{ht_m}$. We construct two circles K_1, K_2 with center at the elastic axis EA and radii R_1, R_2, $0 < R_1 < R_2$ so that the airfoil is lying inside the circle K_1. The interior of the circle K_1 is moving in vertical direction and rotates around the elastic axis as a solid body together with the airfoil. The exterior of K_2 is not deformed, and in the area between K_1 and K_2 we use an interpolation. First, we define the mapping $\mathbf{H}_{t_m}(X_1, X_2)$, where $\boldsymbol{X} = (X_1, X_2) \in \Omega_{h0}$, describing the vertical motion and rotation:

$$\mathbf{H}_{t_m}(X_1, X_2) = \begin{pmatrix} \cos\alpha(t_m) & \sin\alpha(t_m) \\ -\sin\alpha(t_m) & \cos\alpha(t_m) \end{pmatrix} \begin{pmatrix} X_1 - X_{EA1} \\ X_2 - X_{EA2} \end{pmatrix} + \begin{pmatrix} X_{EA1} \\ X_{EA2} \end{pmatrix} + \begin{pmatrix} 0 \\ -H(t_m) \end{pmatrix},$$

where (X_{EA1}, X_{EA2}) represents the position of the elastic axis at time $t = 0$. If we denote the identical mapping by $\mathbf{Id}(X_1, X_2) = (X_1, X_2)$, we define the mapping $\overline{\mathrm{A}}_{t_m}$ as a combination of $\mathbf{Id}$ and $\mathbf{H}_{t_m}$:

$$\bar{\mathrm{A}}_{t_m}(X_1, X_2) = (1 - \xi)\mathbf{H}_{t_m}(X_1, X_2) + \xi\mathbf{Id}(X_1, X_2), \tag{10.46}$$

where

$$\xi = \xi(\hat{r}) = \min\left(\max\left(0, \frac{\hat{r} - R_1}{R_2 - R_1}\right), 1\right) \tag{10.47}$$

and $\hat{r} = \sqrt{(X_1 - X_{EA1})^2 + (X_2 - X_{EA2})^2}$ is the distance of a point $\boldsymbol{X} \in \Omega_{h0}$ from the elastic axis.

In the case of the space-time DGM it is necessary to construct the ALE mapping for all time instants in the intervals I_m. To this end, we introduce the mapping by the formula

$$\bar{\mathrm{A}}_t(\boldsymbol{X}) = \frac{t_m - t}{\tau_m}\bar{\mathrm{A}}_{t_{m-1}}(\boldsymbol{X}) + \frac{t - t_{m-1}}{\tau_m}\bar{\mathrm{A}}_{t_m}(\boldsymbol{X}), \quad t \in I_m, \ \boldsymbol{X} \in \Omega_{h0}. \tag{10.48}$$

Since the mapping $\bar{\mathrm{A}}_t$ is nonlinear, the elements from the initial triangulation $\mathcal{T}_{h0}$ would be transformed by this mapping to curved elements. Therefore, the ALE mapping A_t is defined as the conforming piecewise linear space interpolation of $\bar{\mathrm{A}}_t$.

The domain velocity is approximated in the BDF method by the formula of order q in the form

$$z^m(x) = \frac{1}{\tau_m}\left(\alpha_0 x + \sum_{l=1}^{q} \alpha_l \mathrm{A}_{t_{m-l}}(\mathrm{A}_{t_m}^{-1}(x))\right) \quad \text{for } x \in \Omega_{ht_m}, \tag{10.49}$$

with coefficients α_l, $l = 0, \ldots, q$, given in Tables 8.2 and 8.3. If $m < q$, then we set $q := m$. In the case of the space-time DGM we use (10.48) and express $z(t)$ in the form

$$z(x,t) = \frac{\mathrm{A}_{t_m}(\mathrm{A}_t^{-1}(x)) - \mathrm{A}_{t_{m-1}}(\mathrm{A}_t^{-1}(x))}{\tau_m}, \qquad t \in I_m, x \in \Omega_{ht}. \tag{10.50}$$

10.2.1.3 Coupling Procedure

In solving the complete fluid-structure interaction problem the following coupling algorithm is used.

0. Prescribe $\varepsilon > 0$—the measure of accuracy in the coupling procedure, and an integer $N \geq 0$—the maximal number of iterations in the coupling procedure.
1. Assume that the approximate solution w_h^k of the discrete flow problem (10.39) or the approximate solution $w_{h\tau}|_{I_k}$ of the discrete problem (10.42) and the corresponding lift force L and torsional moment M computed from (10.44) and (10.45) are known.
2. Extrapolate linearly L and M from the interval $[t_{k-1}, t_k]$ to $[t_k, t_{k+1}]$. Set $n := 0$.
3. *Prediction of* H, α: Compute the displacement H and angle α at time t_{k+1} as the solution of system (10.43). Denote it by H^*, α^*.
4. On the basis of H^*, α^* determine the position of the airfoil at time t_{k+1}, the domain $\Omega_{ht_{k+1}}$, the ALE mapping $\mathrm{A}_{ht_{k+1}}$ and the domain velocity z_h^{k+1}.
5. Solve the discrete problem (10.39) at time t_{k+1} or the discrete problem (10.42) in the interval I_{k+1}.
6. *Correction of* H, α: Compute L, M from (10.44) and (10.45) at time t_{k+1} and interpolate L, M in the interval $[t_k, t_{k+1}]$. Compute H, α at time t_{k+1} from (10.43).
7. If $|H^* - H| + |\alpha^* - \alpha| \geq \varepsilon$ and $n < N$, set $H^* = H$, $\alpha^* = \alpha$, $n := n + 1$ and go to 4. Otherwise, $k := k + 1$ and go to 2.

If $N = 0$, then the coupling of the flow and structural problems is weak (loose). With increasing N and decreasing ε, the coupling becomes strong.

10.2.1.4 Numerical Examples

In order to demonstrate the applicability and robustness of the developed methods numerical tests were performed. Here we present the results of computations

carried out for the flow around the NACA 0012 profile with the following data: $m = 0.086622\,\mathrm{kg}$, $S_a = -0.000779673\,\mathrm{kg\,m}$, $I_a = 0.000487291\,\mathrm{kg\,m^{-2}}$, $k_{HH} = 105.109\,\mathrm{N\,m^{-1}}$, $k_{\alpha\alpha} = 3.696682\,\mathrm{N\,m\,rad^{-1}}$, $d_{HH} = 0.0\ \mathrm{N\,s\,m^{-1}}$, $d_{\alpha\alpha} = 0.0\,\mathrm{N\,m\,s\,rad^{-1}}$, $\mu = 1.72 \cdot 10^{-5}\,\mathrm{kg\,m^{-1}\,s^{-1}}$, far-field pressure $p = 101{,}250\,\mathrm{Pa}$, far-field density $\rho = 1.225\,\mathrm{kg\,m^{-3}}$, Poisson adiabatic constant $\gamma = 1.4$, specific heat $c_v = 721.428\ \mathrm{m^2\,s^{-2}\,K^{-1}}$, heat conduction coefficient $k = 2.428 \cdot 10^{-2}\,\mathrm{kg\,m\,s^{-2}\,K^{-1}}$, airfoil length $c = 0.3\,\mathrm{m}$, airfoil depth $l = 0.05\,\mathrm{m}$, initial conditions for the structural equations $H(0) = -20\,\mathrm{mm}$, $\alpha(0) = 6°$, $\dot{H}(0) = \dot{\alpha}(0) = 0$. The computations started at a time instant $t = -\delta < 0$ with a fixed airfoil. Then at time $t = 0$ the airfoil was released and the FSI process followed.

For the space discretization quadratic polynomials ($p = 2$) were used. In the case of the BDF time discretization, the second-order approximation was used (we denote it by BDF-DGp2q2). In the case of the ST-DG method the quadratic polynomials in space and linear polynomials in time were used (denoted by ST-DGp2q1). For both methods the SIPG variant of the viscous terms was used (i.e., $\Theta = 1$). In the penalty form $\hat{\boldsymbol{J}}_h^\sigma$ the weight σ was defined by (9.67) with the parameter $C_W = 500$ in the interior part of the penalty form, whereas $C_W = 5000$ in the boundary penalty, in order to obtain an accurate approximation of the Dirichlet boundary conditions. The time step is defined as $\tau = 0.003299\,c/v_\infty$ s, where $c = 0.3\,\mathrm{m}$ is the length of the airfoil and v_∞ is the magnitude of the far-field velocity. The constants in the artificial viscosity forms were chosen $\nu_1 = \nu_2 = 0.1$.

With the use of the triangulation at time $t = 0$ shown in Fig. 10.2, low Mach number flow was computed for far-field velocities 20 and 37.5 m/s. The results are shown in Figs. 10.3 and 10.4. We can see that both methods DG-BDF (full lines) and ST-DG (dashed lines) give very similar results. In the case of the far-field velocity 20 m/s the airfoil vibrations are damped. The velocity 37.5 m/s leads already to flutter, when the vibrations are damped no longer. Our results are comparable with computations presented in [179], where the Taylor–Hood finite element method was applied to the model based on the incompressible Navier–Stokes equations.

In the second example, the described methods are applied to the numerical simulation of airfoil vibrations induced by high-speed hypersonic flow with large Reynolds

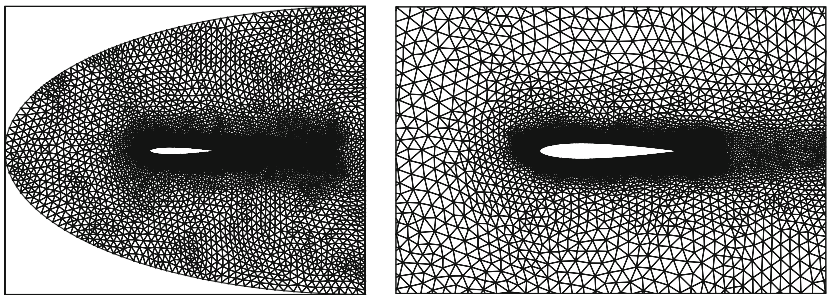

Fig. 10.2 Triangulation at time $t = 0$ with 17,158 elements used for computing subsonic flow and its detail near the airfoil

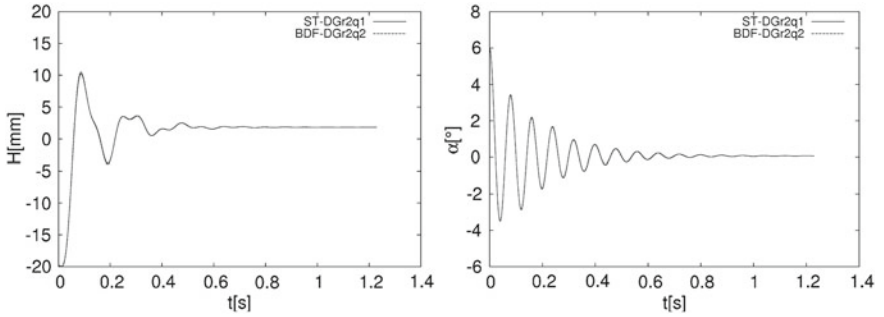

Fig. 10.3 Displacement and rotation angle of the airfoil in dependence on time for far-field velocity 20 m/s and far-field Mach number $M_\infty = 0.0588$

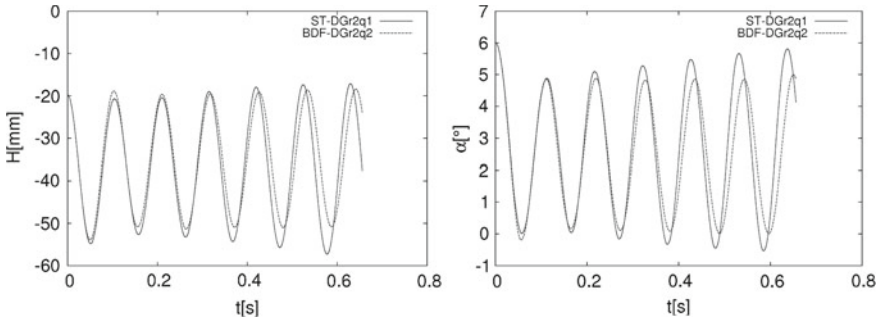

Fig. 10.4 Displacement and rotation angle of the airfoil in dependence on time for far-filed velocity 37.5 m/s and far-field Mach number $M_\infty = 0.1102$

numbers. It appears that in the method combining the DG space discretization with the BDF time discretization some instabilities may appear for flows with far-field Mach numbers higher than 1.5. This is not the case of the ST-DG method, which is very robust and stable for a large range of the Mach and Reynolds numbers.

Here we present the results of the simulation of airfoil vibrations induced by the flow with far-field Mach number $M_\infty = 3$ and Reynolds numbers $\mathrm{Re} = 10^4$ and 10^5 computed using the initial triangulation shown in Fig. 10.5. In this case damped airfoil vibrations were obtained for the same data as above except for bending and torsional stiffnesses, which were now 1000 times higher that before. Figure 10.6 shows the Mach number distribution in the vicinity of the airfoil at several time instants. One can see well resolved oblique shock wave, shock waves leaving the trailing edge and wake. The presented results were computed by the system of programs worked out by J. Česenek [45].

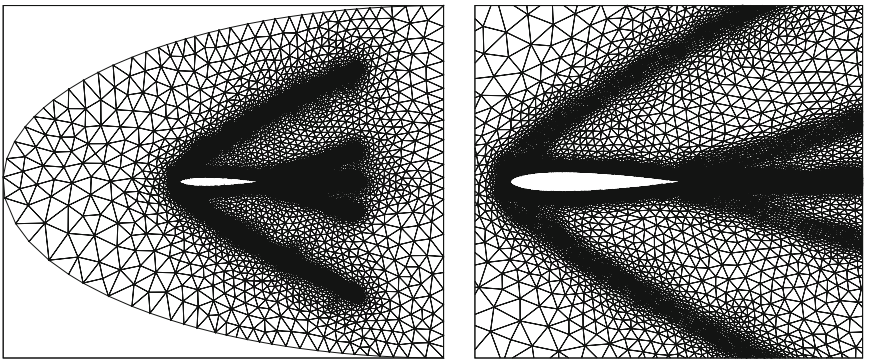

Fig. 10.5 Triangulation at time $t = 0$ with 42,821 elements used for computing hypersonic flow and its detail near the airfoil

10.2.2 Interaction of Compressible Flow and an Elastic Body

In this section, the interaction of compressible flow with an elastic body will be solved. We use the model of dynamical linear elasticity formulated in a bounded open set $\Omega^b \subset \mathbb{R}^2$ representing the elastic body, which has a common boundary with the reference domain Ω_0 occupied by the fluid at the initial time. By $\boldsymbol{u}(X,t) = (u_1(X,t), u_2(X,t))$, $X = (X_1, X_2) \in \overline{\Omega}^b$, $t \in [0,T]$, we denote the displacement of the body.

10.2.2.1 Dynamical Elasticity Equations

The equations describing deformation of the elastic body Ω^b have the form

$$\rho^b \frac{\partial^2 u_i}{\partial t^2} + C\rho^b \frac{\partial u_i}{\partial t} - \sum_{j=1}^{2} \frac{\partial \tau_{ij}^b}{\partial X_j} = 0 \quad \text{in } \Omega^b \times (0,T), \quad i = 1,2. \tag{10.51}$$

Here ρ^b denotes the material density and τ_{ij}^b, $i, j = 1, 2$, are the components of the stress tensor defined by the generalized Hooke's law for isotropic bodies in the form

$$\tau_{ij}^b = \lambda^b \nabla \cdot \boldsymbol{u}\, \delta_{ij} + 2\mu^b e_{ij}^b(\boldsymbol{u}), \quad i, j = 1,2. \tag{10.52}$$

By $\boldsymbol{e}^b = (e_{ij}^b)_{i,j=1}^2$ we denote the strain tensor defined by

$$e_{ij}^b(\boldsymbol{u}) = \frac{1}{2}\left(\frac{\partial u_i}{\partial X_j} + \frac{\partial u_j}{\partial X_i}\right), \quad i, j = 1,2. \tag{10.53}$$

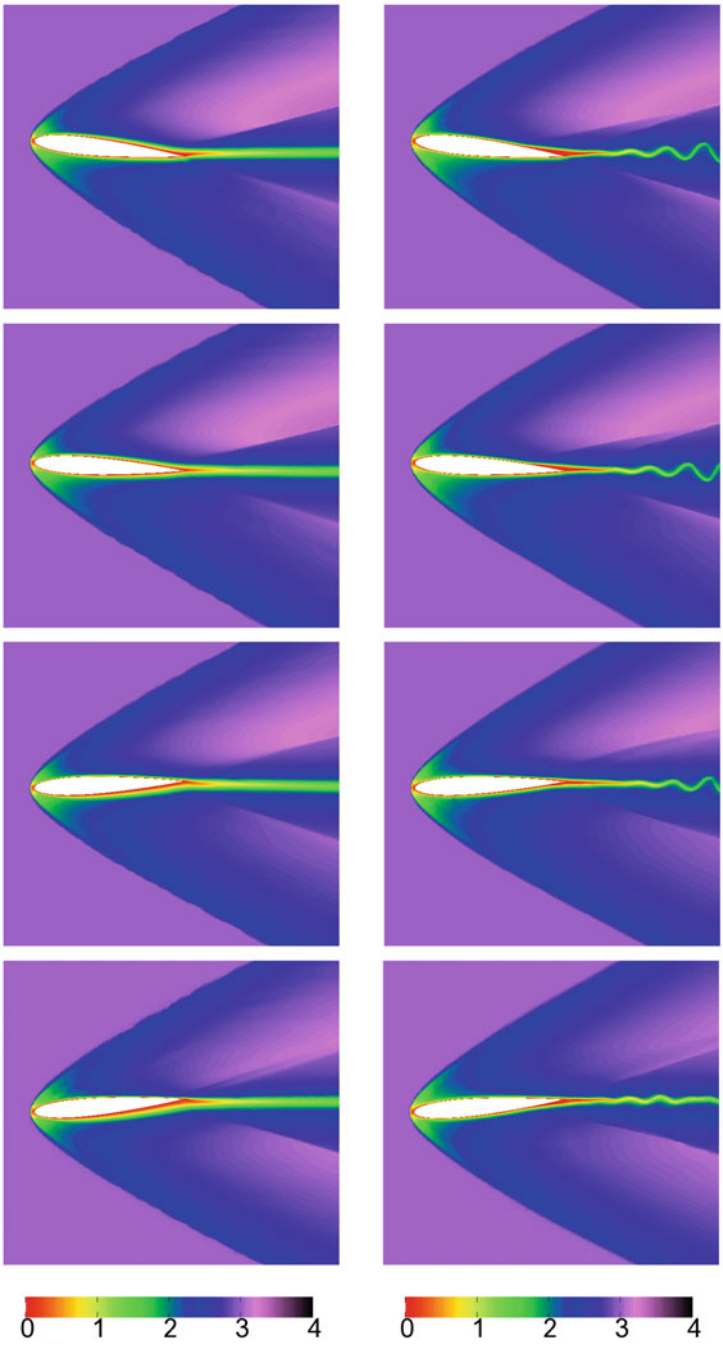

Fig. 10.6 Mach number distribution at time instants $t = 0.0, 0.00039, 0.00078, 0.00117$ s for the far-field velocity 1020 m/s ($M_\infty = 3.0$) and Reynolds numbers Re $= 10^4$ (*left*) and Re $= 10^5$ (*right*)

The Lamé coefficients λ^b and μ^b are related to the Young modulus E^b and the Poisson ratio σ^b:

$$\lambda^b = \frac{E^b \sigma^b}{(1+\sigma^b)(1-2\sigma^b)}, \quad \mu^b = \frac{E^b}{2(1+\sigma^b)}. \tag{10.54}$$

The expression $C\rho^b \frac{\partial u_i}{\partial t}$, where $C \geq 0$, is the dissipative structural damping of the system.

We complete the elasticity problem by initial and boundary conditions. The initial conditions read as

$$\boldsymbol{u}(\cdot, 0) = 0, \quad \frac{\partial \boldsymbol{u}}{\partial t}(\cdot, 0) = 0, \quad \text{in } \Omega^b. \tag{10.55}$$

Further, we assume that $\partial\Omega^b = \overline{\Gamma}^b_W \cup \overline{\Gamma}^b_D$, where Γ^b_W and Γ^b_D are two disjoints parts of $\partial\Omega^b$. ($\overline{\Gamma}^b_W$ and $\overline{\Gamma}^b_D$ denote their closures in $\partial\Omega$.) We assume that Γ^b_W is a common part between the fluid and structure at time $t = 0$. This means that $\Gamma^b_W \subset \partial\Omega_{W_0}$. On Γ^b_W we prescribe the normal component of the stress tensor and assume that the part Γ^b_D is fixed. This means that the following boundary conditions are used:

$$\sum_{j=1}^{2} \tau^b_{ij} n_j = T^n_i \quad \text{on } \Gamma^b_W \times (0, T), \quad i = 1, 2, \tag{10.56}$$

$$\boldsymbol{u} = 0 \quad \text{on } \Gamma^b_D \times (0, T). \tag{10.57}$$

By $\boldsymbol{T}^n = (T^n_1, T^n_2)$ we denote the prescribed normal component of the stress tensor.

The structural problem consists in finding the displacement $\boldsymbol{u}$ satisfying equations (10.51) and the initial and boundary conditions (10.55)–(10.57).

10.2.2.2 Formulation of the FSI Problem

Now we come to the formulation of the coupled FSI problem. We denote the common boundary between the fluid and the structure at time t by $\tilde{\Gamma}_{W_t}$. Thus,

$$\tilde{\Gamma}_{W_t} = \left\{ x \in \mathbb{R}^2;\ x = X + \boldsymbol{u}(X, t),\ X \in \Gamma^b_W \right\} \subset \partial\Omega_{W_t}. \tag{10.58}$$

We see that the shape of the domain Ω_t is determined by the displacement $\boldsymbol{u}$ of the part Γ^b_W at time t. The ALE mapping A_t will be constructed with the aid of a special stationary linear elasticity problem in Sect. 10.2.2.4.

If the domain Ω_t occupied by the fluid at time t is known, we can solve the problem describing the flow, and compute the surface force acting onto the body on the interface $\tilde{\Gamma}_{W_t}$, which can be transformed to the reference configuration, i.e., to the

interface Γ_W^b. In case of the linear elasticity model, when only small deformations are considered, we use the transmission condition

$$\sum_{j=1}^{2} \tau_{ij}^b(X) n_j(X) = \sum_{j=1}^{2} \tau_{ij}^f(x) n_j(X), \quad i = 1, 2, \tag{10.59}$$

where τ_{ij}^f are the components of the aerodynamic stress tensor of the fluid, i.e.,

$$\tau_{ij}^f = -\mathrm{p}\delta_{ij} + \tau_{ij}^V, \quad i, j = 1, 2, \tag{10.60}$$

the points x and X satisfy the relation

$$x = X + \boldsymbol{u}(X, t), \quad X \in \Gamma_W^b, \ x \in \tilde{\Gamma}_{W_t}, \tag{10.61}$$

and $\boldsymbol{n}(X) = (n_1(X), n_2(X))$ denotes the outer unit normal to the body Ω^b on Γ_W^b at the point X. Here we consider the dimensional quantities: p is dimensional pressure and τ_{ij}^V is the viscous part of the aerodynamic stress tensor defined by the dimensional velocity in (9.8):

$$\tau_{ij}^V = \mu \left(\frac{\partial v_i}{\partial x_j} + \frac{\partial v_j}{\partial x_i} \right) + \lambda \nabla \cdot \boldsymbol{v}\, \delta_{ij}, \quad i, j = 1, \ldots, 2. \tag{10.62}$$

Further, the fluid velocity is determined on the moving part of the boundary $\tilde{\Gamma}_{W_t}$ by the second transmission condition

$$\boldsymbol{v}(x, t) = \boldsymbol{z}_D(x, t) := \frac{\partial \boldsymbol{u}(X, t)}{\partial t}. \tag{10.63}$$

The points x and X satisfy relation (10.61).

Now we formulate the *continuous FSI problem*: We want to determine the domain Ω_t, $t \in (0, T]$, and functions $\boldsymbol{w} = \boldsymbol{w}(x, t)$, $x \in \overline{\Omega_t}$, $t \in [0, T]$ and $\boldsymbol{u} = \boldsymbol{u}(X, t)$, $X \in \overline{\Omega}^b$, $t \in [0, T]$, satisfying Eqs. (10.4), (10.51), the initial conditions (10.6), (10.55), the boundary conditions (10.7)–(10.9), (10.57) and the transmission conditions (10.59), (10.63).

Theoretical analysis of qualitative properties of this problem, as the existence, uniqueness and regularity of its solution, is open. In what follows, we describe a method for the numerical solution of the elasticity problem.

10.2.2.3 Discrete Structural Problem

The space semidiscretization of the structural problem will be carried out by the conforming finite element method. By Ω_h^b we denote a polygonal approximation of

the domain Ω^b. We construct a triangulation $\mathcal{T}_h^b$ of the domain Ω_h^b formed by a finite number of closed triangles with the following properties:

(a) $\overline{\Omega}_h^b = \bigcup_{K\in\mathcal{T}_h^b} K$.
(b) The intersection of two different elements $K, K' \in \mathcal{T}_h^b$ is either empty or a common edge of these elements or their common vertex.
(c) The vertices lying on $\partial\Omega_h^b$ are lying on $\partial\Omega^b$.
(d) The set $\overline{\Gamma}_W^b \cap \overline{\Gamma}_D^b$ is formed by vertices of some elements $K \in \mathcal{T}_h^b$.

Further, by Γ_{Wh}^b and Γ_{Dh}^b we denote the parts of $\partial\Omega_h^b$ approximating Γ_W^b and Γ_D^b.

The approximate solution of the structural problem will be sought in the finite-dimensional space $\boldsymbol{X}_h = X_h \times X_h$, where

$$X_h = \left\{ v_h \in C(\overline{\Omega}_h^b);\ v_h|_K \in P_s(K),\ \forall K \in \mathcal{T}_h^b \right\} \tag{10.64}$$

and $s \geq 1$ is an integer. In $\boldsymbol{X}_h$ we define the subspace $\boldsymbol{V}_h = V_h \times V_h$, where

$$V_h = \left\{ y_h \in X_h;\ y_h|_{\overline{\Gamma}_{Dh}^b} = 0 \right\}. \tag{10.65}$$

Deriving the space semidiscretization can be obtained in a standard way. Multiplying Eq. (10.51) by any test function $y_{hi} \in V_h$, $i = 1, 2$, integrating over Ω_h^b, applying Green's theorem and using the boundary condition (10.56), we obtain an identity containing the form

$$a_h^b(\boldsymbol{u}_h, \boldsymbol{y}_h) = \int_{\Omega_h^b} \lambda^b \nabla\cdot\, \boldsymbol{u}_h \nabla\cdot\, \boldsymbol{y}_h \,\mathrm{d}X + 2\int_{\Omega_h^b} \mu^b \sum_{i,j=1}^{2} e_{ij}^b(\boldsymbol{u}_h)\, e_{ij}^b(\boldsymbol{y}_h)\,\mathrm{d}X, \tag{10.66}$$

defined for $\boldsymbol{u}_h = (u_{h1}, u_{h2})$, $\boldsymbol{y}_h = (y_{h1}, y_{h2}) \in \boldsymbol{X}_h$. Moreover, we set

$$(\boldsymbol{\varphi}, \boldsymbol{\psi})_{\Omega_h^b} = \int_{\Omega_h^b} \boldsymbol{\varphi}\cdot\boldsymbol{\psi}\,\mathrm{d}X, \quad (\boldsymbol{\varphi}, \boldsymbol{\psi})_{\Gamma_{Wh}^b} = \int_{\Gamma_{Wh}^b} \boldsymbol{\varphi}\cdot\boldsymbol{\psi}\,\mathrm{d}S. \tag{10.67}$$

We use the approximation $\boldsymbol{T}_h^n \approx \boldsymbol{T}^n$ and the notation $\boldsymbol{u}_h'(t) = \frac{\partial \boldsymbol{u}_h(t)}{\partial t}$ and $\boldsymbol{u}_h''(t) = \frac{\partial^2 \boldsymbol{u}_h(t)}{\partial t^2}$. Then we define the *approximate solution of the structural problem* as a mapping $t \in [0, T] \to \boldsymbol{u}_h(t) \in \boldsymbol{V}_h$ such that there exist the derivatives $\boldsymbol{u}_h'(t)$, $\boldsymbol{u}_h''(t)$ and the identity

$$(\rho^b \boldsymbol{u}_h''(t), \boldsymbol{y}_h)_{\Omega_h^b} + (C\rho^b \boldsymbol{u}_h'(t), \boldsymbol{y}_h)_{\Omega_h^b} + a_h^b(\boldsymbol{u}_h(t), \boldsymbol{y}_h) = (\boldsymbol{T}_h^{\boldsymbol{n}}(t), \boldsymbol{y}_h)_{\Gamma_{Wh}^b},$$
$$\forall\, \boldsymbol{y}_h \in \boldsymbol{V}_h, \quad \forall t \in (0, T), \tag{10.68}$$

and the initial conditions

$$\boldsymbol{u}_h(X,0)=0,\quad \boldsymbol{u}_h'(X,0)=0,\quad X\in\Omega_h^b. \tag{10.69}$$

are satisfied.

The discrete problem (10.68), (10.69) is equivalent to the solution of a system of ordinary differential equations. Let functions $\varphi_1,\dots,\varphi_m$ form a basis of the space V_h. Then the system of the $n=2m$ vector functions

$$(\varphi_1,0),\dots,(\varphi_m,0),\quad (0,\varphi_1),\dots,(0,\varphi_m)$$

forms a basis of the space $\boldsymbol{V}_h=V_h\times V_h$. Let us denote them by $\boldsymbol{\varphi}_1,\dots\boldsymbol{\varphi}_n$. Then the approximate solution $\boldsymbol{u}_h$ can be expressed in the form

$$\boldsymbol{u}_h(t)=\sum_{j=1}^{n} p_j(t)\boldsymbol{\varphi}_j,\quad t\in[0,T]. \tag{10.70}$$

Let us set $\boldsymbol{p}(t)=(p_1(t),\dots,p_n(t))^T$. Using $\boldsymbol{\varphi}_i,\ i=1,\dots,n$, as test functions in (10.68), we get the following system of ordinary differential equations

$$\mathbb{M}\boldsymbol{p}''=\boldsymbol{G}-\mathbb{S}\boldsymbol{p}-C\mathbb{M}\boldsymbol{p}', \tag{10.71}$$

where $\mathbb{M}=(m_{ij})_{i,j=1}^n$ is the mass matrix and $\mathbb{S}=(s_{ij})_{i,j=1}^n$ is the stiffness matrix with the elements $m_{ij}=(\rho^b\boldsymbol{\varphi}_j,\boldsymbol{\varphi}_i)_{\Omega_h^b}$ and $s_{ij}=a_h^b(\boldsymbol{\varphi}_j,\boldsymbol{\varphi}_i)$, respectively. The aerodynamic force vector $\boldsymbol{G}=\boldsymbol{G}(t)=(G_1(t),\dots,G_n(t))^T$ has the components $G_i(t)=(\boldsymbol{T}_h^n(t),\boldsymbol{\varphi}_i)_{\Gamma_{Wh}^b},\ i=1,\dots,n$. System (10.71) is equipped with the initial conditions

$$p_j(0)=0,\quad p_j'(0)=0,\quad j=1,\dots,n. \tag{10.72}$$

One possibility for solving the discrete initial value problem (10.71), (10.72) is the application of the Newmark method [69], which is popular in solving elasticity problems. We consider the partition of the time interval $[0,T]$ formed by the time instants $0=t_0<t_1<\cdots<t_r=T$ introduced in Sect. 10.1.2. Let us set $\boldsymbol{p}_0=0, \boldsymbol{z}_0=0, \boldsymbol{G}_k=\boldsymbol{G}(t_k)$, and introduce the approximations $\boldsymbol{p}_k\approx\boldsymbol{p}(t_k)$ and $\boldsymbol{q}_k\approx\boldsymbol{p}'(t_k)$ for $k=1,2,\dots,r$. The Newmark scheme can be written in the form

$$\begin{aligned}\boldsymbol{p}_{k+1}=\boldsymbol{p}_k+\tau_k\boldsymbol{q}_k+\tau_k^2\Big(&\beta\left(\mathbb{M}^{-1}\boldsymbol{G}_{k+1}-\mathbb{M}^{-1}\mathbb{S}\boldsymbol{p}_{k+1}-C\boldsymbol{q}_{k+1}\right)\\&+\left(\frac{1}{2}-\beta\right)\left(\mathbb{M}^{-1}\boldsymbol{G}_k-\mathbb{M}^{-1}\mathbb{S}\boldsymbol{p}_k-C\boldsymbol{q}_k\right)\Big),\end{aligned} \tag{10.73}$$

$$\boldsymbol{q}_{k+1} = \boldsymbol{q}_k + \tau_k \Big(\gamma \left(\mathbb{M}^{-1} \boldsymbol{G}_{k+1} - \mathbb{M}^{-1} \mathbb{S} \boldsymbol{p}_{k+1} - C \boldsymbol{q}_{k+1} \right) + (1-\gamma) \left(\mathbb{M}^{-1} \boldsymbol{G}_k - \mathbb{M}^{-1} \mathbb{S} \boldsymbol{p}_k - C \boldsymbol{q}_k \right) \Big), \tag{10.74}$$

where $\beta, \gamma \in \mathbb{R}$ are parameters. From Eq. (10.74) we get

$$\boldsymbol{q}_{k+1} = \frac{1}{1 + C\gamma\tau_k} \Big(\boldsymbol{q}_k + \tau_k \Big(\gamma \left(\mathbb{M}^{-1} \boldsymbol{G}_{k+1} - \mathbb{M}^{-1} \mathbb{S} \boldsymbol{p}_{k+1} \right) + (1-\gamma) \left(\mathbb{M}^{-1} \boldsymbol{G}_k - \mathbb{M}^{-1} \mathbb{S} \boldsymbol{p}_k - C \boldsymbol{q}_k \right) \Big) \Big). \tag{10.75}$$

The substitution of (10.75) into (10.73) yields the relation

$$\begin{aligned} \boldsymbol{p}_{k+1} = \boldsymbol{p}_k + \tau_k \boldsymbol{q}_k + \beta \tau_k^2 \Big(& \mathbb{M}^{-1} \boldsymbol{G}_{k+1} - \mathbb{M}^{-1} \mathbb{S} \boldsymbol{p}_{k+1} - \frac{C}{1 + C\gamma\tau_k} \boldsymbol{q}_k \\ & - \frac{C\gamma\tau_k}{1 + C\gamma\tau_k} \left(\mathbb{M}^{-1} \boldsymbol{G}_{k+1} - \mathbb{M}^{-1} \mathbb{S} \boldsymbol{p}_{k+1} \right) \\ & - \frac{C\tau_k}{1 + C\gamma\tau_k} (1-\gamma) \left(\mathbb{M}^{-1} \boldsymbol{G}_k - \mathbb{M}^{-1} \mathbb{S} \boldsymbol{p}_k - C \boldsymbol{q}_k \right) \Big) \\ & + \left(\frac{1}{2} - \beta \right) \tau_k^2 \left(\mathbb{M}^{-1} \boldsymbol{G}_k - \mathbb{M}^{-1} \mathbb{S} \boldsymbol{p}_k - C \boldsymbol{q}_k . \right. \end{aligned}$$

This implies that

$$\begin{aligned} \boldsymbol{p}_{k+1} = \boldsymbol{p}_k + \tau_k \boldsymbol{q}_k - C\xi_k \boldsymbol{q}_k + \xi_k \left(\mathbb{M}^{-1} \boldsymbol{G}_{k+1} - \mathbb{M}^{-1} \mathbb{S} \boldsymbol{p}_{k+1} \right) \\ + \left(\left(\frac{1}{2} - \beta \right) \tau_k^2 - C (1-\gamma) \xi_k \tau_k \right) \left(\mathbb{M}^{-1} \boldsymbol{G}_k - \mathbb{M}^{-1} \mathbb{S} \boldsymbol{p}_k - C \boldsymbol{q}_k \right), \end{aligned}$$

which can be written in the form

$$\begin{aligned} \left(\mathbb{I} + \xi_k \mathbb{M}^{-1} \mathbb{S} \right) \boldsymbol{p}_{k+1} = \boldsymbol{p}_k + (\tau_k - C\xi_k) \boldsymbol{q}_k + \xi_k \mathbb{M}^{-1} \boldsymbol{G}_{k+1} \\ + \left(C (\gamma - 1) \xi_k \tau_k + \left(\frac{1}{2} - \beta \right) \tau_k^2 \right) \left(\mathbb{M}^{-1} \boldsymbol{G}_k - \mathbb{M}^{-1} \mathbb{S} \boldsymbol{p}_k - C \boldsymbol{q}_k \right). \end{aligned} \tag{10.76}$$

Here we use the notation

$$\xi_k = \beta \tau_k^2 \left(1 - \frac{C\gamma\tau_k}{1 + C\gamma\tau_k} \right) = \frac{\beta \tau_k^2}{1 + C\gamma\tau_k}. \tag{10.77}$$

If $\boldsymbol{p}_k$ and $\boldsymbol{q}_k$ are known, then $\boldsymbol{p}_{k+1}$ is obtained from system (10.76) and afterwards $\boldsymbol{q}_{k+1}$ is computed from (10.75).

In numerical examples presented in Sect. 10.2.2.6, the parameters $\beta = 1/4$ and $\gamma = 1/2$ were used. This choice yields the second-order Newmark method.

10.2.2.4 Construction of the ALE Mapping for Fluid

The ALE mapping A_t is constructed with the aid of an artificial stationary elasticity problem. We seek $\boldsymbol{d} = (d_1, d_2)$ defined in Ω_0 as a solution of the elastostatic system

$$\sum_{j=1}^{2} \frac{\partial \tau_{ij}^a}{\partial x_j} = 0 \quad \text{in } \Omega_0, \quad i = 1, 2, \tag{10.78}$$

where τ_{ij}^a are the components of the *artificial stress tensor*

$$\tau_{ij}^a = \lambda^a \nabla \cdot \boldsymbol{d}\, \delta_{ij} + 2\mu^a e_{ij}^a, \quad e_{ij}^a(\boldsymbol{d}) = \frac{1}{2}\left(\frac{\partial d_i}{\partial x_j} + \frac{\partial d_j}{\partial x_i}\right), \quad i, j = 1, 2. \tag{10.79}$$

The artificial Lamé coefficients λ^a and μ^a are related to the artificial Young modulus E^a and to the artificial Poisson ratio σ_a in a similar way as in (10.54). On the boundary $\partial\Omega_{t_0}$ conditions for $\boldsymbol{d}$ are prescribed by

$$\boldsymbol{d}|_{\partial\Omega_i \cup \partial\Omega_o} = 0, \ \boldsymbol{d}|_{\Gamma_{W_0} \setminus \Gamma_W} = 0, \ \boldsymbol{d}(X, t) = \boldsymbol{u}(X, t), \ X \in \Gamma_W. \tag{10.80}$$

The solution of problem (10.78)–(10.80) gives us the ALE mapping of $\overline{\Omega}_0$ onto $\overline{\Omega}_t$ in the form

$$\mathrm{A}_t(X) = X + \boldsymbol{d}(X, t), \quad X \in \overline{\Omega}_0, \tag{10.81}$$

for each time t.

Problem (10.78)–(10.80) is discretized by conforming piecewise linear finite elements on the mesh $\mathcal{T}_{h0}$ used for computing the flow field in the beginning of the computational process in the polygonal approximation Ω_{h0} of the domain Ω_0. We introduce the finite element spaces

$$\mathcal{X}_h = \{\boldsymbol{d}_h = (d_{h1}, d_{h2}) \in (C(\overline{\Omega}_{0h}))^2; \ d_{hi}|_K \in P_1(K) \ \forall K \in \mathcal{T}_{h0}, \ i = 1, 2\},$$
$$\mathcal{V}_h = \{\boldsymbol{\varphi}_h \in \mathcal{X}_h; \ \boldsymbol{\varphi}_h(Q) = 0 \text{ for all vertices } Q \in \partial\Omega_{0h}\}, \tag{10.82}$$

and the form

$$B_h(\boldsymbol{d}_h, \boldsymbol{\varphi}_h) = \left((\lambda^a + \mu^a)\nabla \cdot \boldsymbol{d}_h, \nabla \cdot \boldsymbol{\varphi}_h\right)_{\Omega_{0h}} + \left(\mu^a \nabla \boldsymbol{d}_h, \nabla \boldsymbol{\varphi}_h\right)_{\Omega_{0h}}. \tag{10.83}$$

Then the approximate solution of problem (10.78), (10.80) is defined as a function $\boldsymbol{d}_h \in \mathscr{X}_h$ satisfying the Dirichlet boundary conditions (10.80) at the vertices on $\overline{\Gamma}_W^b$ and the identity

$$B_h(\boldsymbol{d}_h, \boldsymbol{\varphi}_h) = 0 \quad \forall \boldsymbol{\varphi}_h \in \mathscr{Y}_h. \tag{10.84}$$

Using linear finite elements is sufficient, because we need only to know the movement of the points of the mesh.

In our computations we choose the Lamé coefficients λ^a and μ^a as constants corresponding to the Young modulus and Poisson ratio $E^a = 10{,}000$ and $\sigma^a = 0.45$.

If the displacement $\boldsymbol{d}_h^{k+1}$ is computed at time t_{k+1}, then in view of (10.81), the approximation of the ALE mapping is obtained in the form

$$\mathrm{A}_{t_{k+1}h}(X) = X + \boldsymbol{d}_h^{k+1}(X), \quad X \in \Omega_{0h}. \tag{10.85}$$

From the ALE mapping at the time instants t_{k-1}, t_k, t_{k+1} it is possible to approximate the domain velocity with the aid of the second-order backward difference formula

$$z_h^{k+1}(x) = \frac{\alpha_{2,0}x - \alpha_{2,1}\mathrm{A}_{t_k h}(\mathrm{A}^{-1}_{t_{k+1}h}(x)) + \alpha_{2,2}\mathrm{A}_{t_{k-1}h}(\mathrm{A}^{-1}_{t_{k+1}h}(x))}{2}, \quad x \in \Omega_{t_{k+1}h}, \tag{10.86}$$

with coefficients $\alpha_{2,0}$, $\alpha_{2,1}$, $\alpha_{2,2}$ from Table 8.3, where we write $k+1$ instead of k.

Remark 10.4 In Sects. 10.2.2.3 and 10.2.2.4, the dynamic elasticity problem was solved with the aid of conforming finite elements used for space discretization and the Newmark method for time discretization. The conforming FEM was also applied to the construction of the ALE mapping. Recently, in works [128, 158, 159, 200–202], all ingredients of the dynamic elasticity discretization and interaction of compressible flow with an elastic body including the construction of the ALE mapping are based on the use of the discontinuous Galerkin method.

10.2.2.5 Coupling Procedure

The realization of the complete fluid-structure interaction problem can be carried out by the following coupling algorithm.

(1) Assume that on time level t_k, the approximate solution $\boldsymbol{w}_h^k$ of the flow problem and the displacement $\boldsymbol{u}_{h,k}$ of the structure are known.

(2) Set $\boldsymbol{u}_{h,k+1}^0 := \boldsymbol{u}_{h,k}$, $l := 1$ and apply the following iterative process:

   (a) Compute the stress tensor τ_{ij}^f and the aerodynamical force acting on the structure and transform it to the interface Γ_{Wh}^b.

(b) Solve the elasticity problem, compute the approximation $\boldsymbol{u}^l_{h,k+1}$ of the displacement at time t_{k+1} and the approximation $\Omega^l_{ht_{k+1}}$ of the flow domain.
(c) Determine the ALE mapping $\mathrm{A}^l_{t_{k+1}h}$ and the approximation $\boldsymbol{z}^l_{h,k+1}$ of the domain velocity.
(d) Solve the flow problem in the domain $\Omega^l_{ht_{k+1}}$.
(e) If the variation of the displacement $|\boldsymbol{u}^l_{h,k+1} - \boldsymbol{u}^{l-1}_{h,k+1}|$ is larger than the prescribed tolerance, go to (a) and $l := l+1$. Else $\boldsymbol{u}_{h,k+1} := \boldsymbol{u}^l_{h,k}$, $k := k+1$ and go to (2).

This algorithm represents the so-called *strong coupling*. If in step (e) we directly set $k := k+1$ and go to (2) already in the case when $l = 1$, then we get the *weak (loose) coupling*.

10.2.2.6 Numerical Example

In order to demonstrate the applicability of the developed method, we present here results of a numerical experiment carried out for a problem modelling the flow in *vocal folds*.

We consider flow through a channel with two bumps which represent time dependent boundaries between the flow and a simplified model of vocal folds. Figure 10.7 shows the situation at the initial time $t = 0$, the flow computational mesh consisting of 5398 elements and the structure computational mesh with 1998 elements. In Fig. 10.8 we see a detail of the channel near the narrowest part of the channel at the initial time and the positions of sensor points used in the analysis.

The numerical experiments were carried out for the following data: magnitude of the inlet velocity $v_{in} = 4\ \mathrm{m\,s^{-1}}$, the fluid viscosity $\mu = 15 \cdot 10^{-6}\,\mathrm{kg\,m^{-1}\,s^{-1}}$, the inlet density $\rho_{in} = 1.225\,\mathrm{kg\,m^{-3}}$, the outlet pressure $p_{out} = 97611$ Pa, the Reynolds number $\mathrm{Re} = \rho_{in} v_{in} H/\mu = 5227$, heat conduction coefficient $k = 2.428 \cdot 10^{-2}\,\mathrm{kg\,m\,s^{-2}\,K^{-1}}$, the specific heat $c_v = 721.428\,\mathrm{m^2\,s^{-2}\,K^{-1}}$, the Poisson adiabatic constant $\gamma = 1.4$. The inlet Mach number is $M_{in} = 0.012$. The Young modulus and the Poisson ratio have values $E^b = 25{,}000$ Pa and $\sigma^b = 0.4$, respectively, the structural damping coefficient is equal to the constant $C = 100\,s^{-1}$

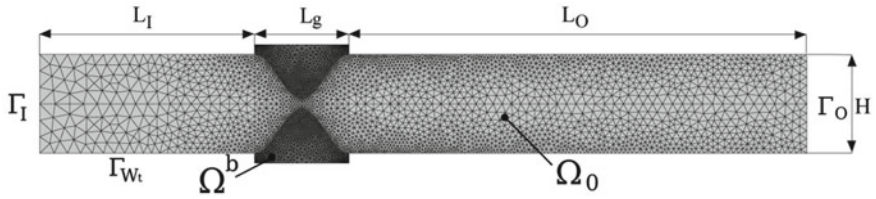

Fig. 10.7 Computational domain at time $t = 0$ with a finite element mesh and the description of its size: $L_I = 50$ mm, $L_g = 15.4$ mm, $L_O = 94.6$ mm, $H = 16$ mm. The width of the channel in the narrowest part is 1.6 mm

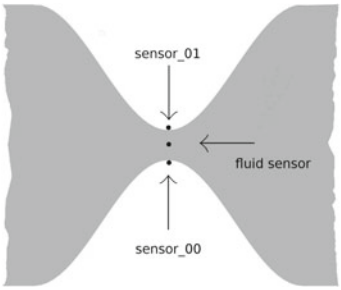

Fig. 10.8 Allocation of the sensors

and the material density $\rho^b = 1040\,\mathrm{kg\,m^{-3}}$. The quadratic ($p = 2$) and linear ($s = 1$) elements were used for the DG-BDF approximation of flow and conforming FE-Newmark approximation of the structural problem, respectively.

We present the results obtained by the fluid-structure interaction computation with the strong coupling. Figure 10.9 shows the velocity isolines in the whole channel at several time instants. In Figs. 10.10 and 10.11 we can see the computational mesh and the velocity field near the vocal folds at several time instants. The maximal velocity is $v \approx 54\ \mathrm{m\ s^{-1}}$. We can observe the *Coanda effect* represented by the attachment

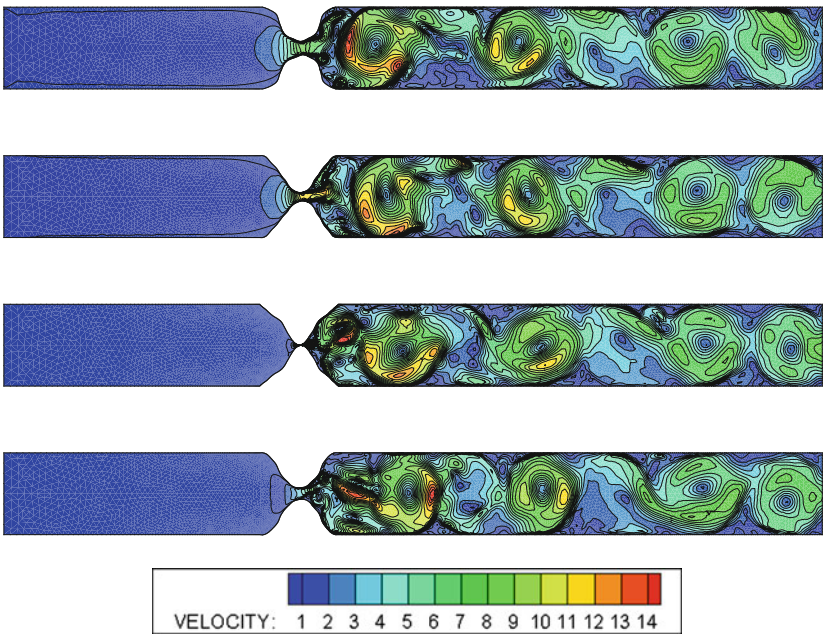

Fig. 10.9 Velocity isolines at time instants $t = 0.1976, 0.1982, 0.1989, 0.1995\,\mathrm{s}$. The legend shows the dimensionless values of the velocity. For getting the dimensional values multiply by $U^* = 4$

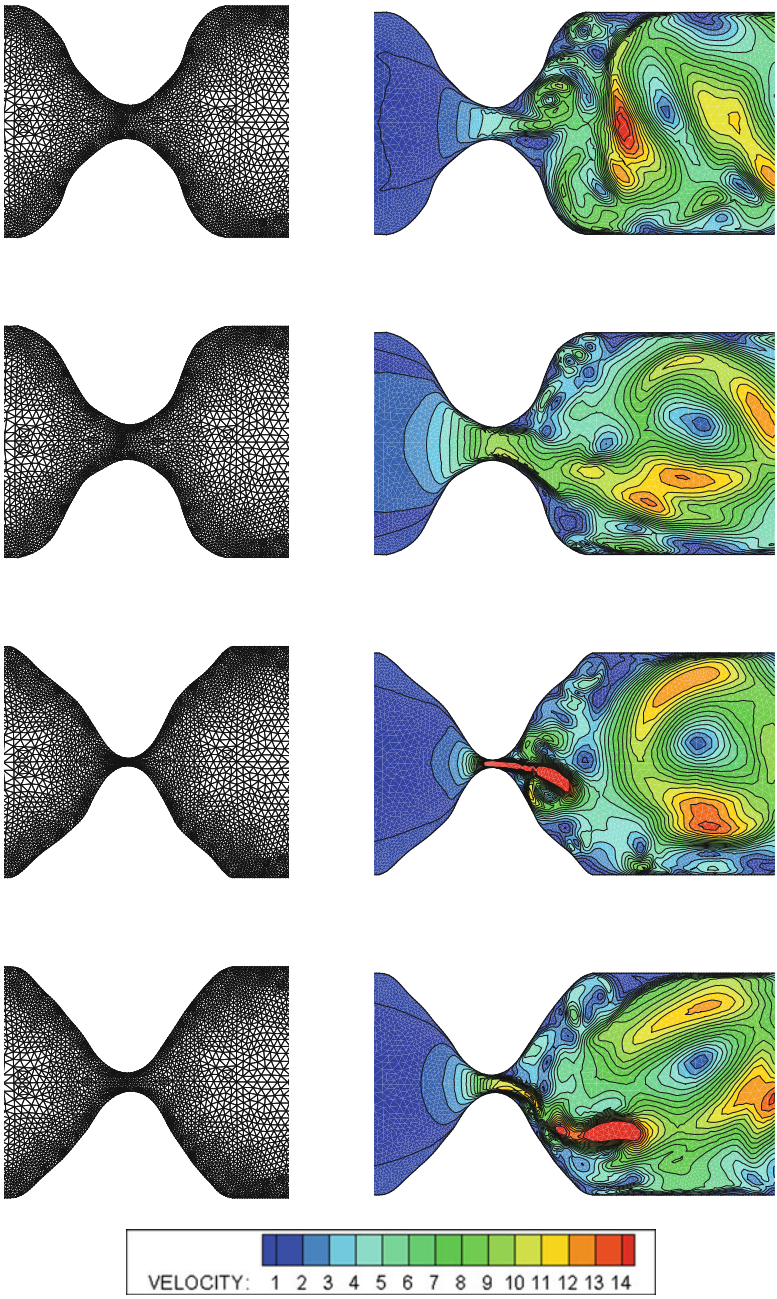

Fig. 10.10 Detail of the mesh and velocity distribution in the vicinity of the narrowest part of the channel at time instants $t = 0.1950,\ 0.1957,\ 0.1963,\ 0.1970\,\mathrm{s}$. The legend shows the dimensionless values of the velocity. For getting the dimensional values multiply by $U^* = 4$

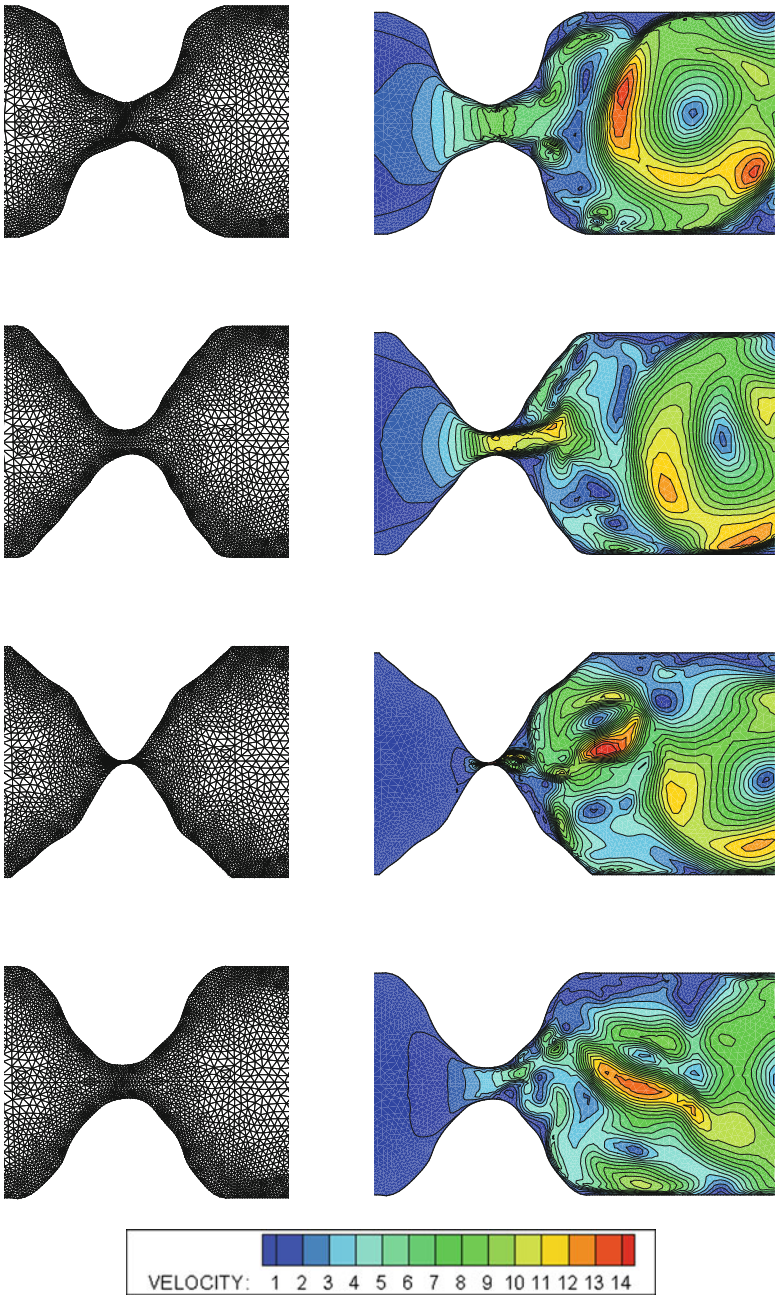

Fig. 10.11 Detail of the mesh and the velocity distribution in the vicinity of the narrowest part of the channel at time instants $t = 0.1976, 0.1982, 0.1989, 0.1995\,\mathrm{s}$. The legend shows the dimensionless values of the velocity. For getting the dimensional values multiply by $U^* = 4$

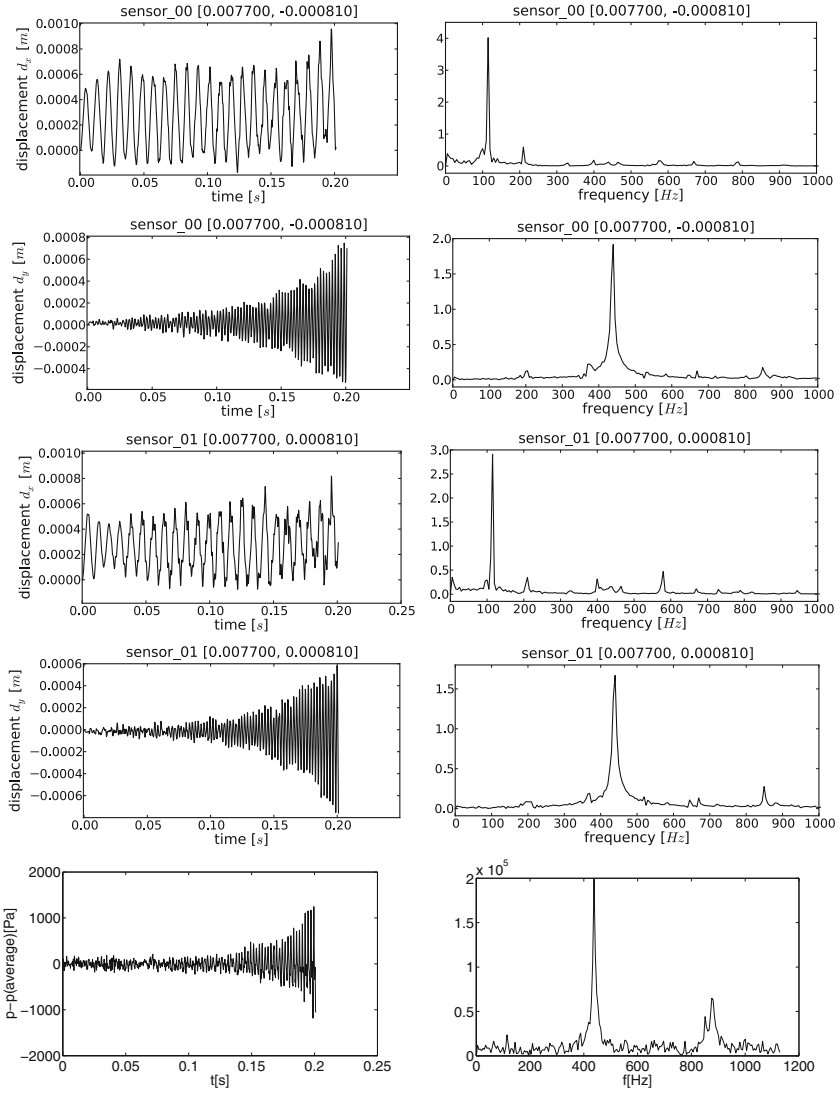

Fig. 10.12 Vibrations of sensor points 00 and 01 on the vocal folds with their Fourier analysis and the fluid pressure fluctuations in the middle of the gap with their Fourier analysis

of the main stream (jet) successively to the upper and lower wall and the formation of large scale vortices behind the vocal folds.

The deformation of vocal folds is tested on two sensor points denoted by 00 and 01 lying on the vocal folds surface shown in Fig. 10.8. The character of the vocal folds vibrations is indicated in Fig. 10.12, which shows the horizontal and vertical displacements d_x and d_y of the sensor points. Moreover, the fluid pressure fluctuations in the middle of the gap as well as the Fourier analysis of the signals are shown. Vocal folds vibrations are not fully symmetric due to the Coanda effect and are composed of the fundamental horizontal mode of vibration with corresponding frequency 113 Hz and by the higher vertical mode with frequency 439 Hz. The increase of vertical vibrations due to the aeroelastic instability of the system results in a fast decrease of the glottal gap. At about $t = 0.2$ s, when the gap was nearly closed, the fluid mesh deformation in this region became too large and the numerical simulation stopped. The dominant peak at 439 Hz in the spectrum of the pressure signal corresponds well to the vertical oscillations of the glottal gap, while the influence of the lower frequency 113 Hz associated with the horizontal vocal folds motion is negligible in the pressure fluctuations. The modeled flow-induced instability of the vocal folds is called *phonation onset* followed in reality by a complete closing of the glottis and consequently by the collisions of vocal folds producing the voice acoustic signal.

http://www.springer.com/978-3-319-19266-6

Discontinuous Galerkin Method
Analysis and Applications to Compressible Flow
Dolejší, V.; Feistauer, M.
2015, XIV, 572 p. 87 illus., 4 illus. in color., Hardcover
ISBN: 978-3-319-19266-6